SHAPE OPTIMIZATION OF MEMS SWITCHES FOR MINIATURIZATION

A THESIS SUBMITTED TO
THE GRADUATE SCHOOL OF NATURAL AND APPLIED SCIENCES
OF
MIDDLE EAST TECHNICAL UNIVERSITY

BY

IMRAN AHMED

IN PARTIAL FULFILLMENT OF THE REQUIREMENTS
FOR
THE DEGREE OF MASTER OF SCIENCE
IN
MECHANICAL ENGINEERING

SEPTEMBER 2018

Approval of the thesis:

SHAPE OPTIMIZATION OF MEMS SWITCHES FOR MINIATURIZATION

submitted by **IMRAN AHMED** in partial fulfillment of the requirements for the degree of **Master of Science in Mechanical Engineering Department, Middle East Technical University** by,

Prof. Dr. Halil Kalıpçılar _____
Dean, Graduate School of **Natural and Applied Sciences**

Prof. Dr. M. A. Sahir Arıkan _____
Head of Department, **Mechanical Engineering**

Assist. Prof. Dr. Hüsnü Dal _____
Supervisor, **Mechanical Engineering Dept., METU**

Assoc. Prof. Dr. Mehmet Ünlü _____
Co-supervisor, **Elec. and Electronics Eng. Dept.,TOBB ETÜ**

Examining Committee Members:

Assist. Prof. Dr. Kıvanç Azgın
Mechanical Engineering Dept., METU _____

Assist. Prof. Dr. Hüsnü Dal
Mechanical Engineering Dept., METU _____

Assoc. Prof. Dr. Mehmet Ünlü
Electrical and Electronics Engineering Dept., TOBB ETÜ _____

Assist. Prof. Dr. Sezer Özerinç
Mechanical Engineering Dept., METU _____

Assist. Prof. Dr. Mert Efe
Metallurgical and Materials Engineering Dept., METU _____

Date: 05/09/2018

I hereby declare that all information in this document has been obtained and presented in accordance with academic rules and ethical conduct. I also declare that, as required by these rules and conduct, I have fully cited and referenced all material and results that are not original to this work.

Name, Last Name: Imran Ahmed

Signature :

ABSTRACT

SHAPE OPTIMIZATION OF MEMS SWITCHES FOR MINIATURIZATION

AHMED, IMRAN
M.S., Department of Mechanical Engineering
Supervisor : Assist. Prof. Dr. Hüsnü Dal
Co-Supervisor : Assoc. Prof. Dr. Mehmet Ünlü

September 2018, 95 pages

This thesis presents miniature optimized cantilever beam MEMS contact switches for low pull-in voltage, low switching time and relatively high contact force for stable switch operation.

Beam based MEMS switches are promising replacements of CMOS based p-i-n diodes and field effect transistor (FET) diode switches due to structural and operation advantages over these solid state switches. High isolation, zero power consumption and very low manufacturing cost are promising advantages compared to solid state switches. In this thesis, optimized miniature shape of gold made MEMS cantilever beam contact switches for low pull-in voltage, small switching time and high contact force have been presented. Low pull-in voltage ensures low power consumption, small switching time facilitates faster operation and high contact force ensures stable operation of switch. Four cantilever beams with thickness 1.6 μm, 1.4 μm, 1.2 μm and 1 μm have been critically analyzed. 11 configurations for each beam based on different length and width have been modeled. A rectangular hole has been introduced at the anchor point of the beam in order to reduce the stiffness of beam which in turn reduces pull-in voltage. Results show that hole at anchor point significantly reduces

stiffness of the beam, and hence pull-in voltage also decreases. It has been also found in this study that, small dimension switch gives high pull-in voltage, small switching time and high contact force whereas large dimension switch gives low pull-in voltage, moderate switching time and low contact force.

The configuration with dimension $22\mu m \times 22\mu m$ has been found as miniature optimized shape of switch with thickness 1.6 μm. This configuration gives pull-in voltage of 35.62 V, contact force of 17.87 μN and switching time of 0.74 μs. In case of switch with thickness 1.4 μm, configuration with dimension $18\mu m \times 18\mu m$ has been found as miniature optimized shape. It gives pull-in voltage of 42.81 V, switching time of 0.59 μs, contact force of 15.60 μN. In case of switches with thickness 1.2 μm and 1 μm , no configuration provides satisfactory results for MEMS application. Any of one criterion from pull-in voltage, switching time and contact force does not satisfy the desired requirement for stable switch operation.

Keywords: MEMS contact switches, Pull-in Voltage, Switching Time, Contact Force, Shape Optimization, MEMS structural analysis.

ÖZ

MEMS ANAHTARLARIN MİNYATÜRLEŞTİRİLMESİ İÇİN ŞEKİL OPTİMİZASYONU

AHMED, IMRAN
Yüksek Lisans, Makina Mühendisliği Bölümü
Tez Yöneticisi : Dr. Öğr. Üyesi Hüsnü Dal
Ortak Tez Yöneticisi : Doç. Dr. Mehmet Ünlü

Eylül 2018 , 95 sayfa

Bu tezde eniyilenmiş minyatür ankastre MEMS kiriş yapısındaki kontak anahtarlarının düşük anahtarlama voltajı, düşük anahtarlama süreleri ve göreceli olarak yüksek kontak kuvvetlerinde stabil çalışması sunulmuştur.

Katı hal anahtarlarına göre yapısal ve işlevsel avantajları sebebiyle kiriş tabanlı MEMS anahtarların CMOS tabanlı p-i-n diyotlar ve Alan Etkili Transistörlerin (AET) yerini alabileceği umut edilmektedir. Yüksek izolasyon, kapalı pozisyonda sıfır güç tüketimi ve çok düşük üretim maliyetleri, MEMS anahtarların, katı hal anahtarlara göre öne çıkan özellikleridir. Bu çalışmada, altından imal edilecek MEMS ankastre kiriş yapısındaki mekanik kontakt tipi anahtların düşük çekme voltajı (anahtarlama voltajı), düşük anahtarlama süresi ve yüksek kontakt kuvveti elde edilebilecek şekilde optimizasyonu üzerine çalışılmıştır. Düşük çekme voltajı düşük enerji tükemi manasına gelmektedir, düşük anahtarlama süresi ise daha hızlı anahtarlama demektir ve yüksek kontakt kuvveti de anahtarlamanın kararlı olmasını sağlar. 1.6 μm, 1.4 μm, 1.2 μm ve 1 μm kalınlıklarda dört adet ankastre kiriş yapısı eleştirel bir bakış açısı ile ele alınıp analiz edilmiştir. Her kiriş 11 değişik boy konfigurasyonunda incelenmiştir. Kirişin

yapısal mukavemetini düşürmek için mesnet noktasında dikdörtgen şeklinde bir delik eklenmiştir, böylelikle çekme voltajı düşürülmüştür. Bu çalışmada, boyutsal olarak küçük olan anahtarların yüksek çekme voltajı, düşük anahtarlama süresi ve yüksek kontakt kuvveti oluşturduğu; boyutsal olarak büyük olan anahtarların ise düşük çekme voltajı, orta seviyede anahtarlama süresi ve düşük kontakt kuvveti doğurduğu gözlemlenmiştir. 1.6 μm kalınlığındaki anahtar için, $22\mu m \times 22\mu m$ şeklindeki konfigürasyon eniyilenmiş anahtar boyutu olarak bulunmuştur. Bu konfigürasyon 35.62 V çekme voltajı, 17.87 μN kontakt kuvveti ve 0.74 μs anahtarlama süresi sağlamaktadır. Kalınlığı 1.4 μm olan anahtar için, $18\mu m \times 18\mu m$ şeklindeki boyut eniyilenmiş konfigürasyon olarak bulunmuştur. Bu konfigürasyon 42.81 V çekme voltajı, 0.59 μs anahtarlama süresi, 15.60 μN kontakt kuvveti doğurmaktadır. Kalınlığı 1.2 μm ve 1 μm olan anahtarlarda hiçbir konfigürasyon tatmin edici sonuçlar vermemektedir. Bu kalınlıklar için bütün kriterler (çekme voltajı, anahtarlama süresi ve kontakt kuvveti) arzu edilen MEMS çalışma parametre sınırlarının dışında çıkmıştır.

Anahtar Kelimeler: MEMS kontakt anahtarları, Çekme Voltajı, Anahtarlama Süresi, Kontakt Kuvveti, Şekil Optimizasyonu, MEMS Yapısal Analizi.

to my parents and family members

ACKNOWLEDGMENTS

I express my heartiest gratefulness to Almighty Allah for his blessings, which enables me to complete this thesis successfully. First and foremost, I would like to express my sincere gratitude and appreciation to my supervisor Assist. Prof. Dr. Hüsnü Dal for his constant support, helpful suggestions and supervision at all stages of this thesis. I would like to express my sincere gratitude and appreciation to my co-supervisor Assoc. Prof. Dr. Mehmet Ünlü for his helpful suggestion and supports during thesis. Despite my slight experience in this field, their scholarly guidance and encouragement influenced me to complete this thesis. I am indebted to them for sharing all their experience and knowledge with me.

It is my pleasure to thank my lab mates Kemal Acikgoz and Yashar Badienia for their immense supports and fruitful knowledge they shared. They were always available to discuss my academic questions regardless of time and condition.

I am deeply grateful to Abdur Rab Raju, Sayed Ahmad Sajib, Delwar Hossain and Zubair Ahmed for their friendship and encouragements during this thesis.

Finally, yet importantly, I would like to express my profound gratitude to my parents and my brother and my sister for their inspirational and mental supports during this thesis. This study would not be finished without their patience and encouragements.

I also would like to thank the Scientific and Technological Research Council of Turkey for their financial support of this research under Grant TUBITAK-315M140 and 116M258.

TABLE OF CONTENTS

LIST OF TABLES

TABLES

LIST OF FIGURES

FIGURES

LIST OF ABBREVIATIONS

MEMS	Micro-Electro Mechanical Systems
FET	Field Effect Transistor
CMOS	Complementary Metal-Oxide Semiconductor
MMIC	Monolithic Microwave Integrated Circuit
IC	Integrated Circuit
DC	Direct Current
AC	Alternating Current
FEA	Finite Element Analysis

CHAPTER 1

INTRODUCTION

1.1 Background and Motivation

At the age of modern technological advance, Micro-Electro Mechanical Systems (MEMS) are gaining much attention and their areas of application are increasing day by day due to their design, fabrication and performance advantages compared to conventional system. MEMS devices can be manufactured at miniature size and light weight with very low fabrication cost. MEMS devices consume low power and can be implemented in complex integrated systems with high reliability and state of the art performances. Nowadays, MEMS devices are being used in myriad of areas such as transportation industry, defense industry, bio-medical applications, aerospace industry, communication systems, consumer electronics etc.

One of the most attractive areas of research in MEMS is MEMS contact switch. MEMS switches have gained tremendous attention from the researchers due to structural and operational advantages compared to p-i-n diodes and Field Effect Transistor (FET) diode switches. MEMS switches consume nearly zero power as they work at 20-80 voltage without consuming current. Therefore it leads to very low power dissipation. Switching energy is 10 nJ to 100 nJ for per cycle. High isolation; low signal leak at off condition, and low insertion loss; low signal loss at on condtion, are desired characteristics in the field of signal processing. MEMS switches show very high isolation and low insertion loss since they are fabricated with air gaps having low capacitance of 2-4fF. MEMS contact switches also show long durability up to 100 billion cycles [1]. High linearity, high shock resistance, wide bandwidth, wider temperature range, low cost, small size and low weight are other remarkable advan-

tages of MEMS contact switches compared to p-i-n diode and FET diode switches [2, 3]. These promising performance criteria have made MEMS contact switches as emerging technology to replace p-i-n diode and FET diode switches in commercial and military applications.

1.2 MEMS Contact Switches

First micro-mechanical switch was developed in 1971 as a cantilever beam actuated electrically. After that, other different types of topologies such as rotary, membrane had been demonstrated successfully [4]. Among all topologies, cantilever beam contact switch gets considerable attentions from researchers due to its minimizing residual stresses effects on mechanical characteristics of switches. From switch contact viewpoint, there are two types of MEMS switches topologies available (i) metal to metal contact and (ii) capacitive coupling.

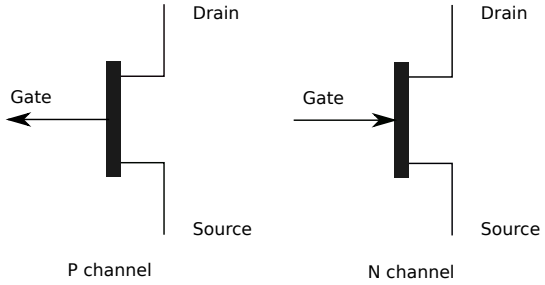

Figure 1.1: Basic structure of FET switch .

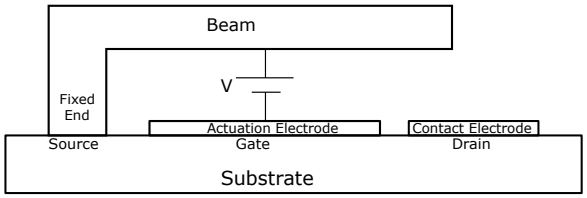

Figure 1.2: Basic structure of cantilever beam MEMS contact switch.

Metal to metal ohmic contact switches provides the opportunity to use it in both low frequency and high frequency applications. This wide-ranging frequency coverage

is one of the prominent advantages of MEMS switches technology [5]. The basic structure of MEMS ohmic contact switches is based on the mechanical cantilever beam or fixed-fixed beam designed in accordance with the existing Complementary Metal-Oxide-Semiconductor (CMOS) based solid state field effect transistor (FET) and p-i-n diodes switches. CMOS based solid state switches consist of three parts as gate, drain and source. MEMS switches also have three parts as beam, actuation electrode and contact electrode. However, MEMS switches use different method to transmit signal. They use mechanical movement based on mechanical beam designed to acquire short circuit or open circuit in integrated electric system or in transmission line. In designing MEMS contact switches, an actuation electrode and a contact electrode are placed right underneath the beam. The whole structure is constructed on substrate. In operation, an increasing DC bias voltage is applied between beam and actuation electrode which generates actuation force. This actuation force pulls down beam and make contact with contact electrode to close the circuit. The performance of MEMS contact switches are evaluated by the three important criteria (i) low pull-in voltage, (ii) low switching time and (iii) moderate contact force. When bias voltage is gradually increased, beam also deforms gradually and reaches a point where deformation becomes unstable. After that, with little increase of bias voltage, beam deforms rapidly and collapses towards the actuation electrode. The bias voltage at which deformation of beam becomes unstable is refereed as pull-in voltage. At unstable situation, electrostatic force surpasses the mechanical restoring force of beam. Low pull-in voltage ensures low operation voltage, hence low power consumption. The contact force is defined as the force which exists between beam and contact electrode during contact phenomenon. A moderate high contact force is essential for stable operation of MEMS switches reminding in mind that the force shall not surpass the limit which causes adhesion or stiction phenomenon between contact electrodes. This adhesion or stiction phenomenon causes failure of switch by preventing break of contact if restoring force of switch is not enough to break the contact between beam and contact electrode. Switching time is defined as the time which is required for the first contact between beam and output contact electrode. Low switching time is another desired characteristics of MEMS contact switches which ensures faster switch operation essential for communication and radar systems .

1.3 MEMS Switch Materials

The reliability and longevity of MEMS switches are directly linked to contact phenomenon between electrodes. To ensure high performance of MEMS contact switches, strict control is required over contact force. In order to have a reliable switch and smotth breaking of electrical contact, contact force lies between μN to mN. Various types of materials have been examined to evaluate the contact performance of MEMS switches. Several properties are given attention to select electrode materials such as low contact resistance, low adhesion, high corrosion resistance, low tendency to form foreign surface films, easy deformability, high signal propagation efficiency etc. Contact resistance shall not be increased beyound 5 Ω. Although preferred contact resistance is below 1 Ω. In this regard, metal to metal contact offers satisfactory contact resistance and superb performance. Considerable number of experiments have proved gold as the best electrode material for high performance MEMS contact switches [6, 7, 5, 8, 9]. Gold based switches create low contact resistance (1-2 Ω) resulting in high contact forces but it has large adhesion forces [10]. Despite high adhesion force, gold based switches are widely used in MEMS contact switches technology due to having good fabrication and technical characteristics. It is easily deformable under low load, it shows high efficient to signal processing, it is highly compatible with Monolithic Microwave Integrated Circuit (MMIC), it is highly non-corrosive material, it can be easily deposited during fabrication processes [11, 12, 13]. These noble characteristics make gold as first choice for micro contact switches.

Different designed cantilever beam MEMS contact switches have been proposed for low pull-in voltage or low switching time or high contact force. Stefanini *et al.* [14] proposed a miniature cantilever MEMS contact switch. They analyzed a cantilever beam MEMS contact switch with dimension $25 \times 25 \mu m$ but the research group did not address the issue of optimization of shape. Nishijima *et al.* [15] and Sedaghat *et al.* [10] proposed a two positions cantilever based MEMS switch to get high contact force and restoring. They used large dimension switch to obtain high contact force and restoring force. Miniaturization, low switching time and high contact force issues were not taken into account. Patel *et al.* [16] analyzed a tether based cantilever beam contact switch to evaluate contact force, pull-in voltage, restoring force. They used a $135 \times 130 \mu m$ dimension switch to obtain high contact force and restoring force.

They did not consider miniaturization issue in their analysis. Low dimension and low weight of MEMS switch are demanding criteria of application for Integrated Circuit (IC) and monolithic microwave integrated circuit(MMIC) since MEMS switch and other electronics structures are built on same substrate. These circuits are widely used in consumer electronics such as cell phone, laptop and digital electronics devices. Nowadays, reduction of weight and dimension are essential requirement for these devices. Therefore, analysis of the switch performance at very small dimension is very essential to address the miniaturization issue in MEMS contact switches.

1.4 Aim of Thesis

The main aim of this thesis is to find out a miniature optimized shape of gold made MEMS cantilever beam contact switch for low pull-in voltage, small switching time and high contact force. Dimension of switch will be considered at minimum level to obtain low pull-in voltage, small switching time and high contact force. Low pull-in voltage ensures low power consumption which is essential for commercial and military applications specially for space or wireless systems. Low stiffness of beam and high actuation force can bring low pull-in voltage but these two conditions require large area and long length beam. However, these two corollaries create trade-off with miniaturization. High contact force ensures stable switch operation. To get high contact force, high actuation voltage is needed to be applied but it raises a trade-off with low power consumption criterion. Hence, an optimized structure of switch is required to solve the problem. Low switching time is required for faster operation such as communication and radar system. High pull-in voltage brings low switching time but it violates the low power consumption criteria. Another technique to decrease switching time is to reduce the mass of beam which leads to a small dimension beam. Therefore, an optimized shape of MEMS switch is needed to find out for the satisfaction of low pull-in voltage, moderate contact force and low switching time criteria simultaneously ensuring small dimension and integrability. To find miniature optimized shape, gold made MEMS cantilever beam contact switches will be critically analyzed. Pull-in voltage, contact force and switching time will be evaluated from simulation and results will be validated with analytic results and literature. Squeeze

film damping effect on switch dynamic behavior will also be evaluated. All results will be compared with literature. After that, a miniature optimized shape will be identified for low pull-in voltage, small switching time and high contact force.

1.5 Outline of Thesis

In chapter 2, information about researches related to different shape of MEMS switch and MEMS switch performance criteria will be given. In chapter 3, mechanical properties of cantilever beam will be discussed. Governing equation of beam, deflection of beam for different applied loads and corresponding stiffness will derived. Finite Element Analysis (FEA) for cantilever beam will be discussed. In chapter 4, electrical mechanisms related to MEMS switches will be elaborately discussed. Analytic equation of actuation force, pull-in voltage, contact force will be derived. Switching time and squeeze film damping will be introduced. In chapter 5, information regarding design criteria of switch will be discussed. Dimensions and properties of MEMS switches will be mentioned. Processes related to evaluation of results will be elaborately discussed. In chapter 6, results will be mentioned and analyzed. Results will be compared with results from various literature. In chapter 7, optimized shape will be identified based on results. Chapter 8 contains the concluding remarks of this thesis and future works.

CHAPTER 2

LITERATURE REVIEW

Various types of MEMS switches; .i.e. cantilever type: fixed-free end cantilever and fixed-fixed end cantilever, diaphragm type: circular type and rectangular type, lateral type and vertical type; have been analyzed to evaluate performance characteristics such as pull-in voltage, switching time, contact resistance, contact force, power handling capacity, isolation and insertion loss. Different modifications have also been proposed by researchers in those cantilever and diaphragm type switches in order to increase switch performance. In this part of thesis, the research works related to this thesis have been critically reviewed.

Considerable number of researchers analyzed the cantilever type switch with and without modifications to investigate the performance criteria. Gold made cantilever beam direct contact switch was investigated by Shalaby *et al.* [17]. In their research, they changed the beam width at anchoring point whereas beam length, thickness and gap between beam and actuation electrode were same as 200 μm, 5 μm and 1.7 μm, respectively. The switch is shown in Figure 2.1.

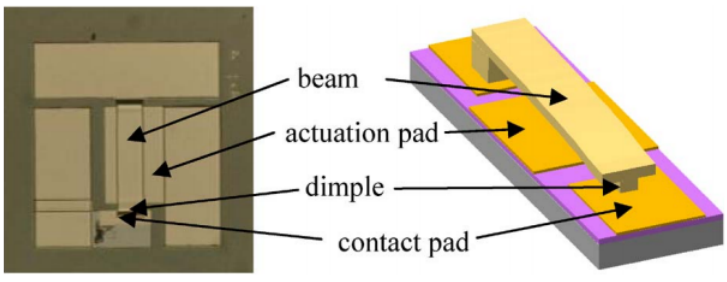

Figure 2.1: Cantilever beam direct contact MEMS switch analyzed by Shalaby *et al.* [17].

They introduced a dimple having width 1.1 μm and height 0.4 μm. They reported that as the beam width at anchoring points increased, stiffness of beam is also increased leading to higher pull-in or pull-down voltage. The corollary of high pull-in voltage was low switching time. Their research also showed that decrease or increase of width of the beam other than anchoring point did not effect pull-in voltage or switching speed. For 64 μm fixed width at anchor point with different width through the length of two beams gave nearly the same pull-down voltage as 27.71 V and 27.65 V and switch opening time was measured as 18.50 μs and 21.31 μs. Again 150 μm fixed width at anchor point with different width through length of two beams gave nearly the same pull-down voltage as 32.01 V and 30.93 V and switch opening time was meandered as 11.16 μs and 12.52 μs. In conclusion, they proposed two rules for cantilever based MEMS contact switches: (i) large actuation area ensures low pull-down voltage and (ii) large width at anchoring point increases pull-in or pull-down voltage which results in low switching speed.

Tether based cantilever beam contact switch was designed and investigated by Patel *et al.* [16] to evaluate contact force, pull-in voltage and restoring force.

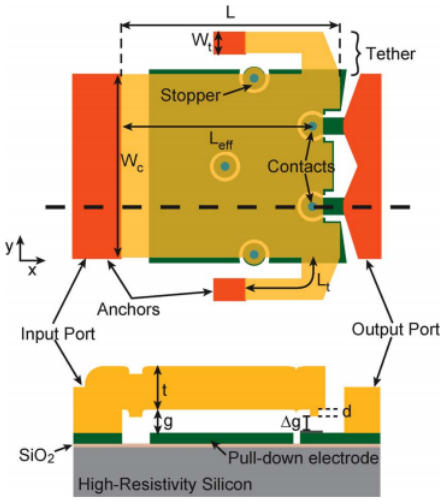

Figure 2.2: Tether based MEMS cantilever beam switch proposed by Patel *et al.* [16].

Results were compared with free cantilever beam. They used two tethers as shown in Figure 2.2. Cantilever beam, tethers and electrode were made of gold. Ruthenium was sputtered on contact electrode to achieve Ru-Au metal contact. Effective length,

width and thickness of the beam were 135 μm, 130 μm and 8 μm. Gap between the bean and the actuation electrode was 0.85 μm. Dimple thickness was 0.3 μm, hence gap between dimple and contact pad 0.55 μm. Pull-in voltage was found 61 V and contact force at 90 actuation volt was found 1.2 mN. Restoring force was found 0.5 mN. They also measured same characteristics of free cantilever beam with identical effective length and width but different thickness of 12 μm. Pull-in voltage was found 64 V and contact force at actuation voltage of 90 V was found 0.8 mN. Restoring force was found 0.49 mN. Switching time was not evaluated in any case. They concluded that use of tethers reduced the effect of residual stress gradient, biaxial stresses and temperature changes during fabrication processes. Residual stresses and temperature changes result in expansion or contraction for cantilever beam. This effects the tip deflection of the beam. Use of tether abated the expansion or contraction of the beam which ensured high performance than free beam.

Nishijima *et al.* [15] analyzed a two position cantilever based MEMS switch. They placed the pull-down electrode near the free end of the beam whereas contact electrode was placed in between the anchor and the pull-down electrode. The switch is depicted in Figure 2.3.

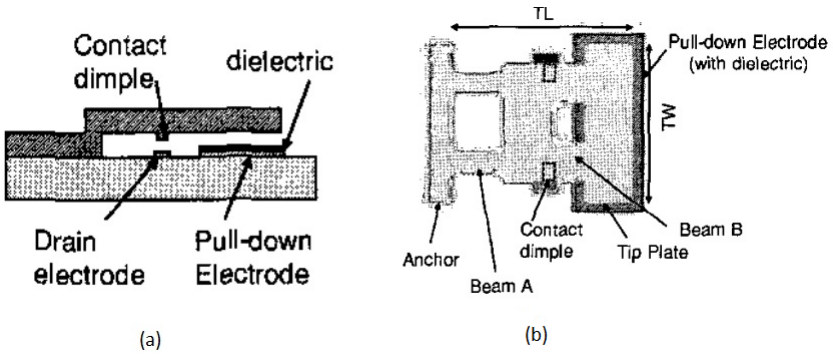

Figure 2.3: Two positions cantilever based MEMS contact switch proposed by Nishijima *et al.* [15]. (a) Cross-section view and (b) top view .

The reason behind the placement of contact electrode in between anchor and pull-down electrode was that it divides beam into two beams: one beam is from the anchor to the dimple portion of the beam and second one is from the dimple to the tip portion of the beam which facilitates parallel spring constant during operation. This increased

contact force and restoring force of the switch. They also introduced a rectangular hole at anchor point. Gold was used to fabricate the cantilever beam switch. The switch dimension was $160\mu m \times 190\mu m$. The gap and thickness of the beam were 1.2 μm and 5 μm. In their study, they found pull in voltage as 12.2-15 V and contact force as 220 μN at 20 V applied voltage. Restoring force was reported as 135 μN. Author did not mention anything about switching time.

Sedaghat *et al.* [10] also proposed a two position cantilever based MEMS switch to get high contact and restoring force. In their design, they placed tow pull-down electrodes underneath the beam at two different positions. Their switch is shown in Figure 2.4.

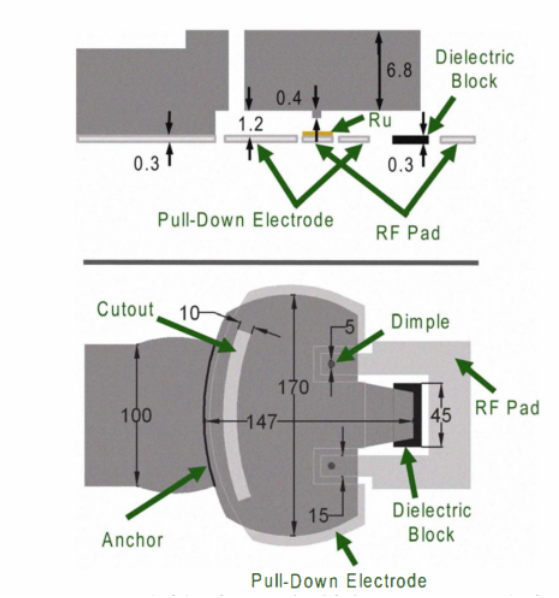

Figure 2.4: Modified two positions cantilever based MEMS switch proposed by Sedaghat *et al.* [10] for high contact and restoring force.

A large pull-down electrode was placed near the anchor and the small pull-down electrode was placed near the free end of the beam. In between these two pull-down electrodes, contact electrode was placed. A dielectric block was placed right underneath the tip of the beam to avoid short circuit. Science behind placing contact electrode in between two pull-down electrodes was that it divides beam into two parts: one is over large pull-down electrode portion and second one is over small pull-down electrode portion of the beam which facilitates variable spring constant effect during operation.

The consequence was high contact force during contact and high restoring force in the absence of voltage. A dimple was fabricated over the contact electrode. The cantilever beam was built of gold and width, length and thickness of beam were 147 μm width, 170 μm and 6.5 μm, respectively. The gap between beam and pull-down electrode was 1.2 μm. They reported that simulated pull-in voltage was 35 V and switching time was below 10 μs. Contact force found from simulation was $120\mu N$ for applied voltage of $55V$ which increased to $760\mu N$ for applied voltage of $70V$. They also experimentally found nearly same results.

Zavracky *et al.* [2, 18] investigated a nickel surface micro-machined cantilever beam micro-switch which is shown in Figure 2.5. To fabricate the switch, they first deposited gold to build beam, then beam was electroplated in nickel plating. Actuation electrode or gate and contact electrode or drain were made of gold. The switch was 65 μm in length, 30 μm in width and 1.8 μm in thickness. Gate was 40 μm in length and 30 μm in width.

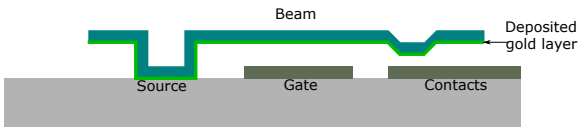

Figure 2.5: Nickel surface micro-machined MEMS cantilever beam switch proposed by Zavracky *et al.* [2, 18].

Gap between beam and gate varied between 1.5 to 1.7 μm and gap between dimple and contact electrode also varied between 0.5 to 0.8 μm. They reported pull threshold or pull-in voltage of 70, 80, 85, 90 and 95 V for different gap. They measured life time more than 10^9 cycles. Authors did not mention anything about switching time and contact force.

Multilayer stack MEMS contact switch was investigated by a number of authors. They analyzed different type of switches such as cantilever beam, diaphragm, etc. A ruthenium-based multilayer stack MEMS contact switch with corrugated SiO_2 /Si_3N_4 diaphragm was investigated by Ke *et al.* [19].

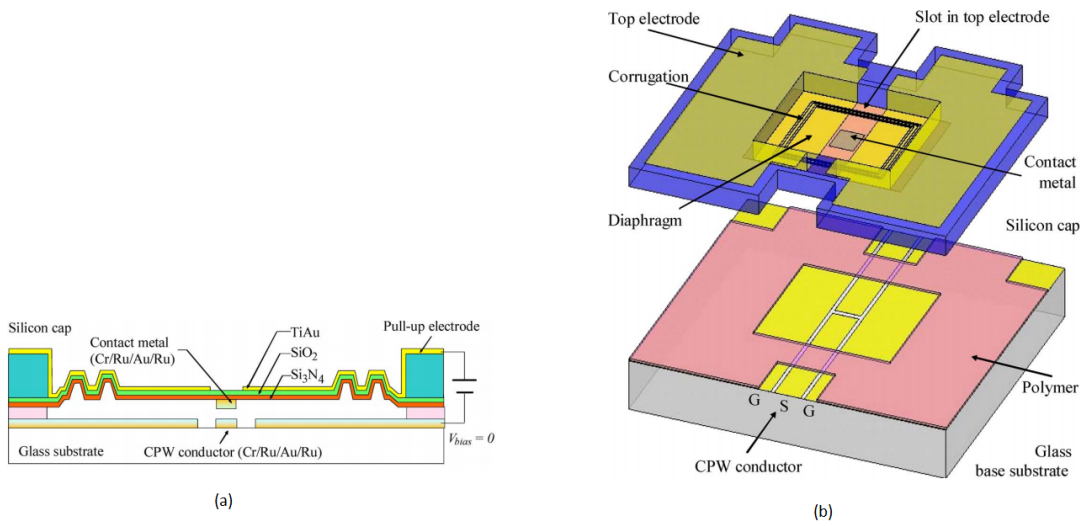

Figure 2.6: Ruthenium-based multilayer stack MEMS contact switch with corrugated silicon dioxide / silicon nitride diaphragm proposed by Ke *et al.* [19]. (a) Cross-section view and (b) schematic view .

They introduced corrugations in diaphragm to reduce the residual stress effect. In their analysis, a chromium/ruthenium/gold/ruthenium (Cr/Ru/Au/Ru) multilayer stack contact area was utilized to evaluate switch performance and compared with Au-Au metal contact switch. The switch is depicted in Figure 2.6. 100 nm SiO_2 /1200 nm Si_3N_4/400 nm TiAu diaphragm was suspended above ground co-planar-wave guide (CPW) signal lines. The CPW lines were built on Pyrex glass wafer by forming 50-nm Cr/50-nm Ru/500-nm Au/50-nm Ru multilayer stack. Diaphragm was 1200 μm at width, 1.7 μm at thickness and 1400 μm at length. Actuation area was $1080 \times 1200 \mu m$. They reported, reduction in pull-in voltage due to introduction of corrugations in diaphragm. Pull-in voltage was reduced from 61 V to 36V and 84 V to 44 V for 5.5 μm and 6.5 μm suspension height of corrugated diaphragm. Their results also showed that Cr/Ru/Au/Ru multilayer stack contacts gave high contact resistance compared with Au-Au metal contact. An actuation voltage of 80 V was required for a stable contact resistance of 700 m Ω for Cr/Ru/Au/Ru contacts but in Au-Au metal contacts, 40 V was required for a stable contact resistance of 300 m Ω.

They reported high switching time compared with cantilever beam switch. Switching time was found as 176 μs.

Hyman *et al.* [20] developed a surface micro-machined and electrostatically actuated cantilever beam contact switch for microwave application. The switch consisted of two armatures principle armature and secondary armature as shown in Figure 2.7. The dimensions of armatures were $20\mu m \times 100\mu m$ and $100\mu m \times 60\mu m$, respectively.

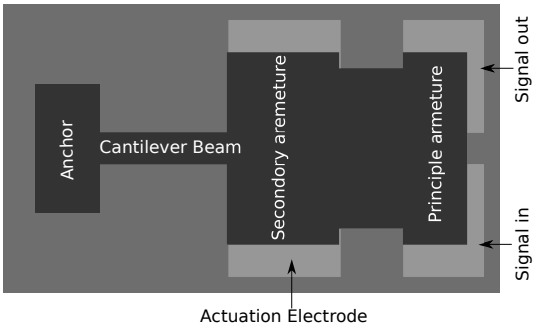

Figure 2.7: MEMS cantilever beam switch proposed by Hyman *et al.* [20].

Thickness of the switch was 3 μm and the beam was fixed at 2 μm height from ground electrode. They reported an actuation voltage of 25 V, a switching time of 20 μs and a contact force of 0.3 mN. Insertion loss was measured to be less than 0.2 dB in the range from DC to 40 GHz and isolation was higher than 50 dB at frequencies below 2 GHz.

Effect of squeeze film damping in MEMS contact switch was investigated by Guo *et al.* [21]. In their study, a gold made cantilever type switch with Au-Au contacts was established.

The schematic view of switch is shown in Figure 2.8, where the values of respective parameters were : $L_1 = 30\mu m$, $L_2 = 24\mu m$, $w_1 = 80\mu m$, $w_2 = 10\mu m$, $w_3 = 16\mu m$, $w_4 = 30\mu m$, $h_1 = 6\mu m$, $h_2 = 0.6\mu m$ and $h_3 = 0.38\mu m$. In their analysis, they found that squeeze film damping force increases the switching operation time as it resisted the closing movement of electrodes and the bouncing off movement after contacts. Simulated pull-in voltage was 65 V whereas measured pull-in voltage was about 63-66 V in their analysis. Switching time for different actuation voltage of 70 V, 74 V and 84 V were reported as 1.62 μs, 1.34 μs and 1.24 μs, correspondingly. Contact force

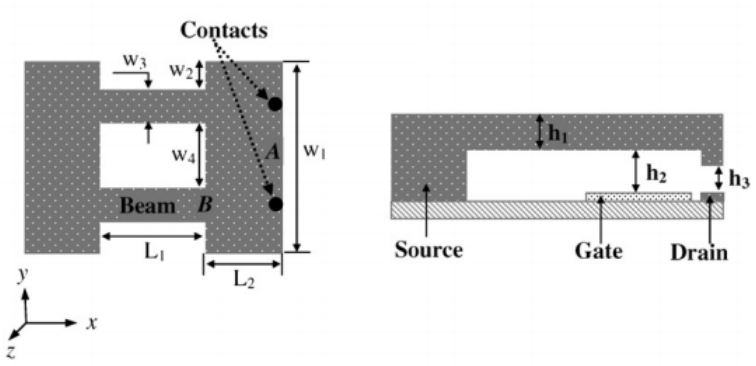

Figure 2.8: Gold made cantilever MEMS switch: top view (left side) and side view (right side) proposed by Guo *et al.* [21].

for same actuation voltages were reported as 27 μN, 44 μN and 78 μN, respectively.

From literature review study, it is clear that no research was conducted thoroughly to find out an optimized shape of MEMS switch for miniaturization purpose and to analyze the MEMS switch's performance at very small dimensions. It is seen from the literature that only low pull-in voltage or low switching time or high contact force was given priority for MEMS switch while small dimension criterion was not taken into account. Different designs were proposed to reduce pull-in voltage and switching time and to increase contact force but miniaturization issue were not addressed. Miniaturization or small dimension of MEMS switches is one of the most demanding criterion for application in different systems specially in integrated circuit (IC) and monolithic microwave integrated circuit(MMIC) which are widely used in consumer electronics. Since it reduces weight and area on IC and MMIC.
This thesis will address miniaturization issue in MEMS contact switch while low pull-in voltage, low switching time and high contact force will be also taken into account simultaneously. For this purpose, an elaborate analysis will be conducted on gold made cantilever beam MEMS contact switch by pushing the dimension of switches at their minimum limit to find out miniature optimized shape. Different designs will be also applied to obtain low pull-in voltage, small switching time and high contact force for stable MEMS applications.

CHAPTER 3

MECHANICAL PROPERTIES OF CANTILEVER BEAM

MEMS switches developed today, even though are at micro scale dimension, still follow the basic mechanical laws. Therefore, in order to comprehend the mechanism of MEMS switchs, first step is to deduce the governing equilibrium equation of cantilever beam and stiffnes of beam. Beam is defined as a three dimensional structural member having one of its dimension is larger than other two and cross section of the beam is normal to the large dimension and varies along this large dimension. Many theories were proposed to analyze the static and dynamic behaviors of beam based on various assumption. Among these theories, Euler-Bernoulli beam theory is widely used. The theory is based on two fundementa assumptions such that cross section of beam deforms insignificantly under loading conditions, i.e. transvese or axial loading, hence considered as rigid and cross section remains perpendicular to the deformed axis of beam [22].

3.1 Governing Equilibrium Equation of Beam

The following assumptions have been considered for the derivation of governing equation of beam.

1. The beam follows hook's law i.e. stress is proportional to strain.

2. Deflection due to shear deformation or shear stress is neglected.

3. Curvature due to deformation is very small.

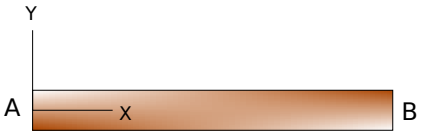

Figure 3.1: Beam

Let us consider a beam AB at its initial unloaded condition when it is straight and horizontal. Now, under the action of a distributed load $q(x)$, the deformed position

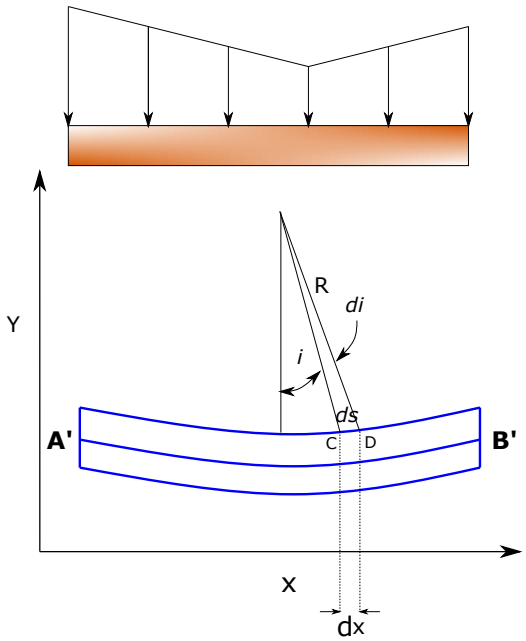

Figure 3.2: Cantilever beam under uniformly distributed load.

of beam is $A'\,B'$ which means that axis of the beam AB gets new position as $A'\,B'$. $A'\,B'$ is called curved axis of beam. Now slop at point C is

$$i = \frac{dy}{dx}. \tag{3.1}$$

According to 3rd assumption, following equation can be read

$$ds = dx = Rdi \tag{3.2}$$

where R is the radius of curvature $A'\,B'$. Combination of equation (3.1) and equation (3.2) leads to,

$$\frac{d^2y}{dx^2} = \frac{1}{R}. \tag{3.3}$$

Again according to simple bending beam theory

$$\frac{1}{R} = \frac{M}{EI} \tag{3.4}$$

where M is moment, E is young modulus, I is first moment of inertia of beam. Now substituting in equation (3.3), moment is found to be:

$$M = EI\frac{d^2y}{d^2x}. \tag{3.5}$$

This is the basic differential equation for deflection of beams. Now let us consider the small part $EFHG$ of deflected beam having length dx. There are reaction forces

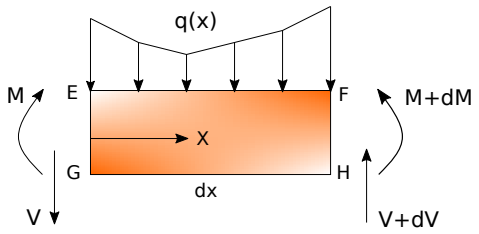

Figure 3.3: Small part of cantilever beam under uniformly distributed load.

acting on the element $EFHG$ due to applied external forces carried out by parts of beam on either side small element $EFHG$. Therefore, the static equilibrium condition of $EFHG$ is

$$V - q(x)dx = V - dV$$

$$q(x) = \frac{dV}{dx} \tag{3.6}$$

where V is share force. Again, moments about any point are also zero for equilibrium. Therefore, moment about G gives

$$(M + dM) + q(x)\frac{dx}{2} = M + Vdx.$$

Neglecting the square of small quantities, V is found as

$$V = \frac{dM}{dx}. \tag{3.7}$$

Now combining equation (3.5), equation (3.6) and equation (3.7), following relation is found

$$EI\frac{d^4y}{d^4x} = q(x) \tag{3.8}$$

which is the governing beam equation for constant EI and distributed load.

3.2 Deflection and Stiffness of Cantilever Beam

Let us consider a cantilever beam shown in Figure 3.4. Now taking moment about XX, M_{xx} is found as

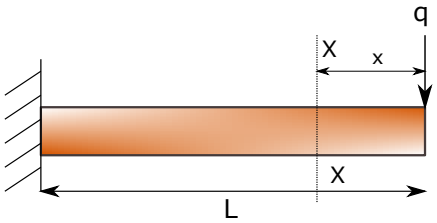

Figure 3.4: Cantilever beam with point load.

$$M_{xx} = EI\frac{d^2y}{d^2x} = -qx. \tag{3.9}$$

Integrating twice,

$$EIy = -\frac{qx^2}{2} + Ax + B. \tag{3.10}$$

Application of boundary conditions $x = L; \frac{dy}{dx} = 0$ and $x = L; y = 0$ in equation (3.10) gives deflection curve equation

$$y = \frac{1}{EI}[-\frac{qx^3}{6} + \frac{qL^2x}{2} - \frac{qL^3}{3}]. \tag{3.11}$$

The above equation provides the deflection of beam at all positions of x and gives maximum deflection at tip of the beam $y_{max} = -\frac{qL^3}{3EI}$ when $x = 0$. Negative sign indicates downward deflection. Then the stiffness of beam due to point load can be calculated as

$$K = \frac{q}{y_{max}} = \frac{Eb}{4}(\frac{t}{L})^3 \tag{3.12}$$

where b and t are width and thickness of beam respectively. Now let us consider another situation where point load is acting at point a instead of the free end. Now taking moment about XX axis,

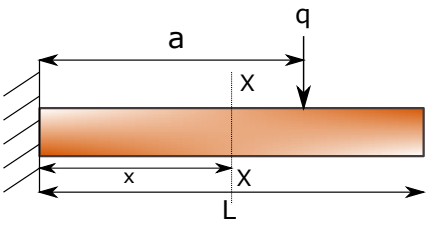

Figure 3.5: Cantilever beam with point load at point a.

$$EI\frac{d^2y}{d^2x} = qx - qa. \tag{3.13}$$

Integrating twice,

$$EIy = \frac{qx^3}{6} - \frac{qax^2}{2} + Ax + B. \tag{3.14}$$

Application of boundary conditions $x = 0; \frac{dy}{dx} = 0$ and $x = 0; y = 0$ in equation (3.14) gives

$$EIy = \frac{qx^3}{6} - \frac{qax^2}{2}. \tag{3.15}$$

Now deflection and slop at distance a are

$$y = -\frac{qa^3}{3EI}$$

$$\frac{dy}{dx} = -\frac{qa^2}{2EI}.$$

Negative sign indicates downward deflection and downward slop. Now the stiffness of beam due to point load at the free end is

$$K = \frac{q}{\frac{qL^3}{3EI}} = \frac{3EI}{L^3}. \tag{3.16}$$

Now the moment beyond distance a is

$$EI\frac{d^2y}{d^2x} = qx - qa - q(x-a)$$

$$EI\frac{d^2y}{d^2x} = 0 \tag{3.17}$$

So there is no moment beyond distance a due to point load at a. Integrating equation (3.17),

$$\frac{dy}{dx} = F \tag{3.18}$$

where F is constant. The equation (3.18) means that from point Z till the free end, slop is identical. Then considering the Figure 3.6, following equation can be written

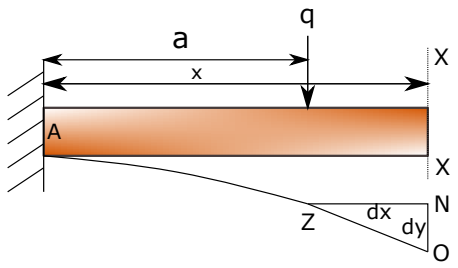

Figure 3.6: Moment of beam beyond distance a .

$$\frac{dy}{dx} = \frac{NO}{NZ} = -\frac{qa^2}{2EI} \tag{3.19}$$

$$NO = -\frac{qa^2}{2EI}NZ = -\frac{qa^2}{2EI}(x-a). \tag{3.20}$$

Now deflection at the free end is the summation of deflection at point Z and O.

$$y = -\frac{qa^3}{3EI} - \frac{qa^2}{2EI}(x-a) = \frac{qa^2}{6EI}(a-3x). \tag{3.21}$$

The equation (3.21) is the generic equation where x indicates the deflection point from fixed end and a indicates acting point of force from fixed end. In MEMS application, force is generally distributed across beams or partially distributed and deflection at free end of beam is considered to evaluate beam stiffness. Now substituting $x = L$, deflection of beam at the free end is found for load at point a. Using principle of superposition, deflection for distributed load across beam is determined by integrating equation (3.21) as

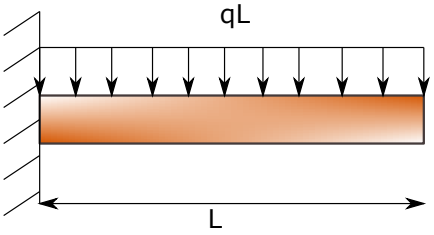

Figure 3.7: Cantilever beam with distributed load.

$$y = \frac{q}{6EI}\int_0^L (a^3 - 3a^2L)da = -\frac{qL^4}{8EI}. \tag{3.22}$$

Now deflection at the free end for partially distributed load from x to L is determined by integrating equation (3.21) as

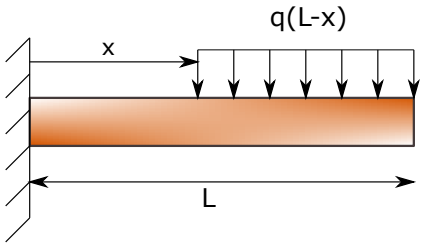

Figure 3.8: Cantilever beam with partially distributed load.

$$y = \frac{qa^2}{6EI}\int_x^L (a - 3L)da. \tag{3.23}$$

$$y = \frac{q}{6EI}(-\frac{3L^4}{4} + Lx^3 - \frac{x^4}{4}). \tag{3.24}$$

The stiffness due to partially distributed load over the beam can be found as

$$K = -\frac{q(L-x)}{y}. \tag{3.25}$$

$$K = -\frac{q(L-x)}{\frac{q}{6EI}(-\frac{3L^4}{4} + Lx^3 - \frac{x^4}{4})}. \tag{3.26}$$

$$K = 2Eb(\frac{t}{L})^3 \frac{1-\frac{x}{L}}{3 - 4(\frac{x}{L})^3 + (\frac{x}{L})^4} \tag{3.27}$$

3.3 Finite Element Formulation for Euler-Bernoulli Beam

In the previous section, the governing fourth order differential equation of Bernoulli beam for constant EI and distributed load $q(x)$ has been found as

$$EI\frac{d^4y}{d^4x} = q(x). \tag{3.28}$$

Now considering the Bernoulli beam element, there are two degree of freedom at each node. Therefore, a cubic polynomial solution which satisfies the homogeneous solution of the above ODE can be written as

$$v(x) = a_1 + a_2x + a_3x^2 + a_4x^3. \tag{3.29}$$

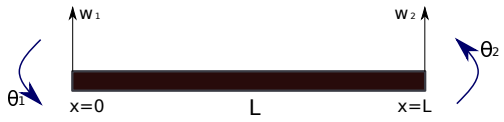

Figure 3.9: Bernoulli beam element with two nodes: where v_1, v_2 are displacements and θ_1, θ_2 are rotations at each node, respectively.

After differentiating $v(x)$,

$$\frac{dv(x)}{dx} = a_2 + 2a_3x + 3a_4x^2. \tag{3.30}$$

Applying nodal conditions, following boundary conditions are obtained

$$v(0) = v_1 = a_1 \tag{3.31}$$

$$\frac{dv(0)}{dx} = \theta_1 = a_2 \tag{3.32}$$

$$v(L) = v_2 = a_1 + a_2L + a_3L^2 + a_4L^3 \tag{3.33}$$

$$\frac{dv(L)}{dx} = \theta_2 = a_2 + 2a_3L + 3a_4L^2. \tag{3.34}$$

Now substituting above equations in equation (3.29), $v(x)$ becomes

$$\begin{aligned} v(x) = &\Big[2(\frac{x}{L})^3 - 3(\frac{x}{L})^2 + 1\Big]v_1 + L\Big[(\frac{x}{L})^3 - 2(\frac{x}{L})^2 + \frac{x}{L}\Big]\theta_1 \\ &+\Big[-2(\frac{x}{L})^3 + 3(\frac{x}{L})^2\Big]v_2 + L\Big[(\frac{x}{L})^3 - (\frac{x}{L})^2\Big]\theta_2. \end{aligned} \tag{3.35}$$

Then

$$\frac{d^2v(x)}{dx^2} = (\frac{12x}{L^3} - \frac{6}{L^2})v_1 + (\frac{6x}{L^2} - \frac{4}{L})\theta_1 + (\frac{6}{L^2} - \frac{12x}{L^3})v_2 + (\frac{6x}{L^2} - \frac{2}{L})\theta_2. \tag{3.36}$$

For discretization of the beam element, displacements can be recast in term of shape function as

$$v(x) = N_1(x)v_1 + N_2(x)\theta_1 + N_3(x)v_2 + N_4(x)\theta_2 \tag{3.37}$$

where $N_i(x)$ is the shape function which consists of interpolation functions

$$\boldsymbol{N} = \begin{bmatrix} N_1(x) & N_2(x) & N_3(x) & N_4(x) \end{bmatrix} \tag{3.38}$$

$$N_1(x) = \frac{1}{L^3}(2x^3 - 3x^2L + L^3)$$
$$N_2(x) = \frac{1}{L^3}(Lx^3 - 2x^2L^2 + L^3x)$$
$$N_3(x) = \frac{1}{L^3}(-2x^3 + 3x^2L)$$
$$N_4(x) = \frac{1}{L^3}(Lx^3 - x^2L^2)$$

and the nodal displacements vector

$$d^T = \begin{bmatrix} w_1 & \theta_1 & w_2 & \theta_2 \end{bmatrix}. \tag{3.39}$$

These polynomial interpolation functions are known as *Hermite cubic interpolation*

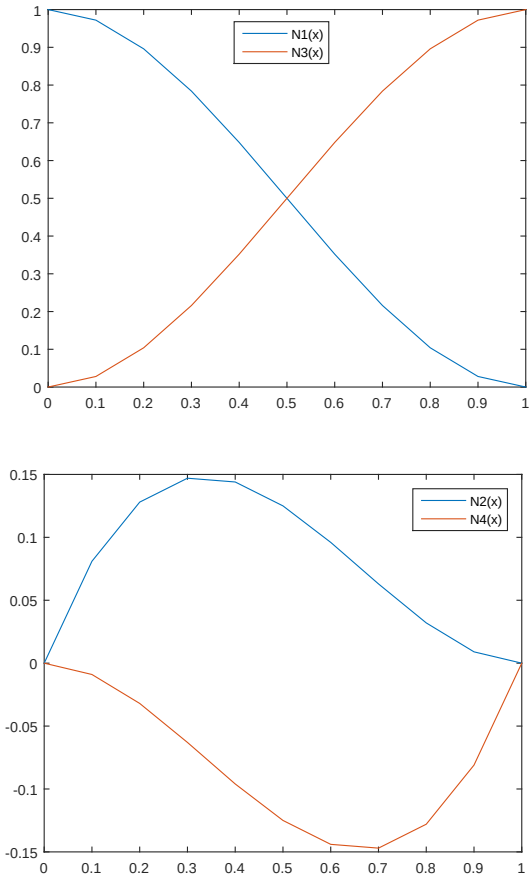

Figure 3.10: Properties of shape functions

function and process the following properties which are also depicted in Figure 3.10

$$N_1(0) = 1, N_1'(0) = 0, N_1(L) = 0, N_1'(L) = 0 \tag{3.40}$$

$$N_2(0) = 0, N_2'(0) = 1, N_2(L) = 0, N_2'(L) = 0 \tag{3.41}$$

$$N_3(0) = 0, N_3'(0) = 0, N_3(L) = 1, N_3'(L) = 0 \tag{3.42}$$

$$N_4(0) = 0, N_4'(0) = 0, N_4(L) = 0, N_4'(L) = 1. \tag{3.43}$$

Hence, the displacement ***v(x)*** can be written as

$$\boldsymbol{v(x)} = [N(x)][d]. \tag{3.44}$$

Recalling from statics that a moment of couple M consists of two opposite forces and this couple M is identical about any axis which is perpendicular to its plane and is zero about any axis existed in its plane. Then couple M about arbitrary z axis, shown in Figure 3.11, can be written as

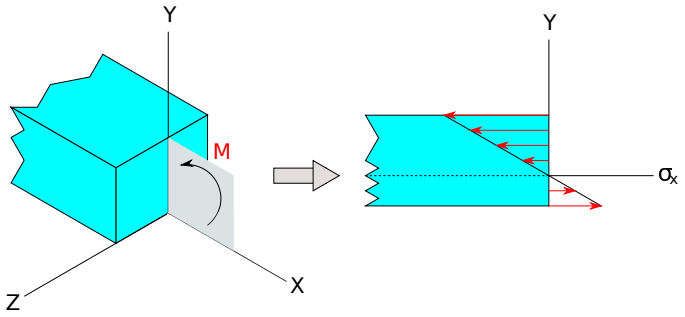

Figure 3.11: Couple M about z-axis.

$$M = \int_A (-y\sigma_x dA). \tag{3.45}$$

Now assuming the material as homogeneous, following equation can be read

$$\sigma_x = E\varepsilon_x \tag{3.46}$$

$$\varepsilon_x = -\frac{y}{R} \tag{3.47}$$

where E is modulus of elasticity and R is the radius of curvature which has been found as $\frac{1}{R} = \frac{d^2v(x)}{dx^2}$. Substitution all in equation (3.45) leads to

$$M = \int_A Ey^2 \frac{d^2v}{dx^2} dA. \tag{3.48}$$

Moment of inertia or second moment of area I is defined as

$$I = \int_A y^2 dA. \tag{3.49}$$

Then combining equation (3.48) and equation (3.49), following equations can be obtained

$$M = EI\frac{d^2v}{dx} \tag{3.50}$$

$$M = EI\kappa \tag{3.51}$$

where $\kappa = \frac{d^2v}{dx^2}$ is called kinematics equation of beam. From the principle of virtual work, it is known know that virtual work done by external force during a virtual displacement δv is

$$\delta w_{int} = \int_V \sigma\varepsilon\delta\varepsilon dV \tag{3.52}$$

$$\delta w_{ext} = \int_V \beta\delta v dV + \int_A f\delta v dA \tag{3.53}$$

$$\delta w_{int} = \delta w_{ext} \tag{3.54}$$

$$\int_V \sigma\varepsilon\delta\varepsilon dV = \int_V \beta\delta v dV + \int_A f\delta v dA \tag{3.55}$$

where

$$\delta w_{int} = \int_V \sigma\varepsilon\delta\varepsilon dV = \text{internal work of internal forces}$$

$$\delta w_{ext} = \int_V \beta\delta v dV + \int_A f\delta v dA = \text{external work of external forces}$$

$$\int_V \beta\delta v dV = \text{work done due to body force}$$

$$\int_A f\delta v dA = \text{work done due to traction or boundary forces.}$$

The principle of virtual work for bending in Bernoulli beam can be written as

$$\int_0^L (M\delta\kappa) = \int_0^L (q(x)\delta v dx) + \int_0^L (\hat{v}\delta v + \hat{M}\delta\theta) \tag{3.56}$$

$$\delta w_{int} = \delta w_{ext}. \tag{3.57}$$

Now combining equation (3.51), equation (3.56) and equation (3.57), following equation is obtained

$$\delta w_{int} = \int_0^L \delta v'' EIv'' dx \tag{3.58}$$

with $\delta\kappa = \delta v''; \kappa = v''$. Applying theses relations in equation (3.44), following equations are found

$$v''(x) = [N(x)]''[d] = [B][d] \tag{3.59}$$

$$\delta v''(x) = [B][\delta d] = [\delta d]^T[B]^T \tag{3.60}$$

where $[B]$ is called strain matrix. With the help of equation (3.58) and equation (3.60), internal virtual work can be expressed as

$$\begin{aligned}\delta w_{int} &= [\delta d]^T[\int_0^L [B]^T EI[B]dx][d] \\ &= [\delta d]^T[k]_e[d]\end{aligned} \tag{3.61}$$

where

$$\begin{aligned}[k]_e &= \int_0^L [B]^T EI[B]dx \\ &= \int_0^L \Big[(\frac{d^2N(x)}{dx^2})^T EI(\frac{d^2N(x)}{dx^2})\Big].\end{aligned} \tag{3.62}$$

Similarly, external virtual work can be read as

$$\begin{aligned}\delta w_{ext} &= [\delta d]^T \int_0^L [[N]^T q(x)dx + [\delta d]^T[f]_{\lceil\sigma}] \\ &= [\delta d]^T[f]_b + [\delta d]^T[f]_{\lceil\sigma}\end{aligned} \tag{3.63}$$

where

$$[f]_b = \int_0^L [N]^T q(x)dx. \tag{3.64}$$

Finally equation (3.57) becomes as

$$[\delta d]^T[k]_e[d] = [\delta d]^T[F]_b + [\delta d]^T[F]_{\lceil\sigma} \tag{3.65}$$

$$[k]_e[d]_e = [f]_b + [f]_{\lceil\sigma}. \tag{3.66}$$

Where

$[k]_e$: Element stiffness matrix for an element having length L

$[d]_e$: Element nodal displacement vectors for an element having length L

$[f]_b$: Element load vectors due to distributed load for an element having length L

$[f]_{\lceil\sigma}$: Element load vectors due to point load for an element having length L.

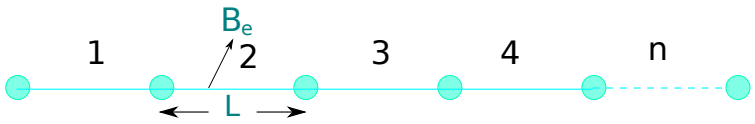

Figure 3.12: Bernoulli beam discretized into n number of element having length L for each element. B_e indicates one element.

Now δw_{int} and δw_{ext} for each element of a structure having length L divided into n number of elements are written as

$$\delta w_{int} = \int_B M\delta\kappa = A_{e=1}^{n} \int_{B_e} M\delta\kappa dx \tag{3.67}$$

$$\delta w_{ext} = \int_B q(x)\delta v dx = A_{e=1}^{n} \int_{B_e} q(x)\delta v dx \tag{3.68}$$

where **A** denotes the standard assembly of discretized n number of local elements. Now the global system assembled from local elements can be defined as

$$[K] = A_{e=1}^{n}[k]_e : \text{Global stiffness matrix}$$

$$[F] = A_{e=1}^{n}[f]_e : \text{Global force vector}$$

$$[D] = A_{e=1}^{n}[d]_e : \text{Global displacement vector}$$

$$[K][D] = [F]. \tag{3.69}$$

Substituting the shape function in equation (3.62) and equation (3.64), the well known nodal stiffness matrix and nodal force vector for Euler-Bernoulli beam element are obtained as

$$k_e = \frac{EI}{L^3}\begin{bmatrix} 12 & 6L & -12 & 6L \\ 6L & 4L^2 & -6L & 2L^2 \\ -12 & -6L & 12 & -6l \\ 6L & 2L^2 & -6L & 4L^2 \end{bmatrix} \tag{3.70}$$

$$f_e = \frac{q(x)L}{12}\begin{bmatrix} 6 \\ L \\ 6 \\ -L \end{bmatrix}. \tag{3.71}$$

CHAPTER 4

ELECTRICAL MECHANISM OF MEMS SWITCH

4.1 MEMS Switches Configurations

Mostly two type of beam structures get much attention for MEMS contact switches applications; they are cantilever beam and fixed-fixed beam or membrane with single or double layer.

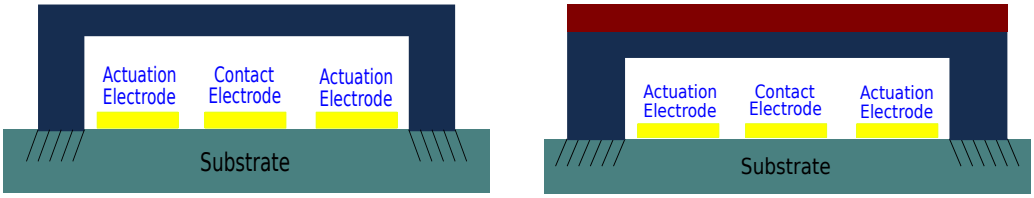

(a) Fixed-Fixed beam MEMS Switch with single layer .

(b) Fixed-Fixed beam MEMS bwitch with double layer.

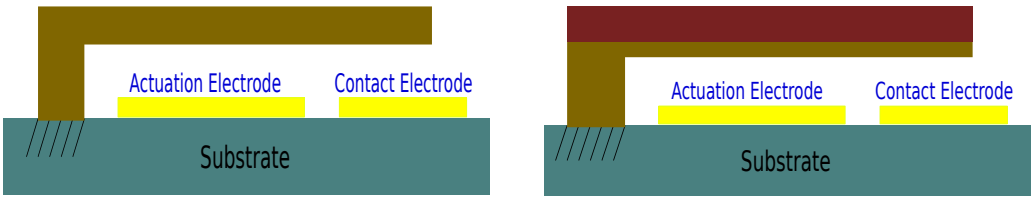

(c) Cantilever beam MEMS switch with single layer.

(d) Cantilever beam MEMS switch with double layer.

Figure 4.1: Different types of beam based MEMS contact switches

In operation, force is applied on beam to bring it at the downstate position to close the circuit to pass signal. MEMS switches consist of two distinct sections. One is actuation section (mechanical) and another one is electrical section. Switches can move

vertically or horizontally based on their application requirements and layout. The force required for mechanical movement is generated by applying different actuation processes such as electrostatic actuation, magnetic actuation and thermal actuation. In electrostatic actuation, a potential difference is applied between the beam and the actuation electrode resulting electrostatic actuation force between the beam and the electrode.

Table 4.1: Different configurations of MEMS switches [23].

Actuation Mechanism						
	Voltage (V)	Current (mA)	Power (mW)	Size	Switching Time (μs)	Contact force (μN)
Electrostatic	30-80	0	0	Small	1-200	50-1000
Thermal	3-5	5-100	0-200	Large	300-10000	500-4000
Magnetic	3-5	20-150	0-100	Medium	300-1000	50-200
Piezoelectric	3-20	0	0	Medium	50-500	50-200

Movement	
Vertical	Typical results in small size devices
Lateral	Typical results in large size devices

Contact Type	
Metal-to-Metal	DC-60 GHz
Capacitive	6-120 GHz

Circuit Configuration	
Series	DC-50 GHz with metal-to-metal contact and low up-state capacitance.
	10-50 GHz with capacitive contact and low up-state capacitance.
Shunt	DC-50 GHz with metal-to-metal contact and low inductance to ground.
	10-200 GHz with capacitive contact and low inductance to ground.

In magnetic actuation, the conductor is placed under the beam and a permanent magnet is placed underneath of the substrate. When current passes through the conductor, magnetic flux of permanent magnet gets changed resulting Lorentz force. This force is used to pull down the beam. In thermal actuator, current is flown through the beam resulting heat dissipation. Heat dissipation expands the beam that reduces the gap between beam and contact electrode gradually. In piezoelectric actuation, a piezoelectric material is placed over the beam. When electric field is applied across the piezoelectric material, mechanical deformation is resulted which reduces the gap between beam and contact electrode gradually. All of these actuation processes have advantages and disadvantages compared to each other. But nowadays electrostatic actuation is commonly used technique in MEMS switches due to its wide range of advantages compared to others such as it ensures high switching speed, consumes low power and is highly compatible with IC assembly. Regarding electric section, a MEMS switch can be positioned in either series or shunt connection as requirements and can be metal to metal contact or capacitive contact switch. The Table 4.1 describes different configurations of MEMS switches used in various applications.

4.2 Electrostatic Actuation Force

When a potential difference is applied between the cantilever beam and the pull-down electrode, an electrostatic force is induced on the beam which pulls the beam downwards out-put electrode. This force is called electrostatic actuation force. To evaluate this actuation force, system is modeled as parallel-plate capacitor. The Figure 4.2 depicts a parallel-plate capacitor with length and width of w and W, respectively. Gap between parallel-plates is g. A time varying voltage source V is applied between two plates. The electric field lines between the beam and the actuation electrode are considered perpendicular, hence fringe effect is neglected. Now the capacitor is charged as

$$Q = C(\eta)V$$

where Q is the charge induced in capacitor, C is the capacitance of capacitor and η is the degree of freedom of movable beam. Since movable plate can only move vertically then η is replaced as g. Now the parallel plate capacitance can be written

as

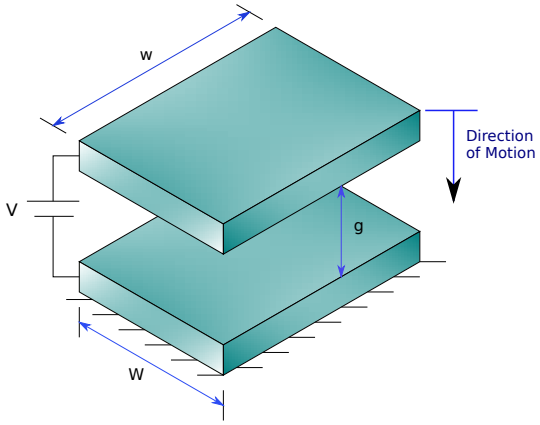

Figure 4.2: Parallel-plate capacitor: when voltage is applied between two plates, upper plate moves downward due to electrostatic force.

$$C(g) = \frac{\varepsilon_o A}{g} = \frac{\varepsilon_o W w}{g} \tag{4.1}$$

where ε_o is the permitting of free space. Then, charge is calculated as

$$Q = C(g)V. \tag{4.2}$$

The potential energy stored in the capacitor is written as

$$E_c = \frac{1}{2}C(g)V^2. \tag{4.3}$$

There are two ways to approximate the electrostatic force between the beam and the actuation electrode: in one way, at first stored co-energy in the capacitor is deduced then electrostatic force is evaluated as the negative gradient of that co-energy [24] and in another way, first the total electric potential energy of battery-capacitor system is derived. Then electrostatic force is evaluated as the negative gradient of the electric potential energy [25]. The second approach has been considered to approximate the electrostatic force in here. When a voltage source is connected to the capacitor, charge Q and electric potential -QV (negative sign since battery losses energy) is induced to the capacitor. Now the potential energy of the battery is reduced to

$$E_b = E_o - QV = E_o - CV^2. \tag{4.4}$$

Then the total potential energy of the battery-capacitor system is

$$E = E_b + E_c = E_o - CV^2 + \frac{1}{2}CV^2 = E_o - \frac{1}{2}CV^2. \tag{4.5}$$

Now according to second approach, the electrostatic force is

$$F_e = -\frac{\partial E(g)}{\partial g} = -\frac{\partial}{\partial g}(E_o - \frac{1}{2}C(g)V^2) = \frac{1}{2}\frac{\partial C(g)}{\partial g}V^2. \tag{4.6}$$

Substitution of $C(g)$ in equation (4.6) leads to

$$F_e = \frac{1}{2}\frac{\partial}{\partial g}(\frac{\varepsilon_o W w}{g})V^2 \tag{4.7}$$

$$F_e = -\frac{1}{2g^2}\varepsilon_o W w V^2 \tag{4.8}$$

The equation (4.8) is analytic form of the actuation force between tow electrodes in MEMS switches application and negative sign indicates attractive nature of force.

4.3 Pull-In Voltage

When a DC potential difference is applied between cantilever the beam and the ground electrode, an electrostatic actuation force is generated between the beam and the electrode which is equally distributed across the actuation area of beam. This actuation force pulls the beam downwards the ground electrode. A restoring mechanical force will resist the downward movement of beam. As a results, a new equilibrium position of beam is reached. With the increase of DC voltage, electrostatic force also increases due to increase of charge. Concurrently, the increased electrostatic force decreases gap between beam and ground electrode which increases capacitance and thus charge and electric field increases as well. Simultaneously, restoring mechanical spring force also increases since deflection of beam at rise. There is a specific DC voltage at which the electrostatic force reaches the restoring mechanical force in magnitude. The DC voltage at which electrostatic force becomes equal to the restoring mechanical spring force is called **pull-in** voltage. Lumped approximation of MEMS switches has been considered as parallel plate actuator system constrained by spring to find pull-in voltage computationally which is shown in Figure 4.3. The governing equation of the 1D lumped mechanical system is given by

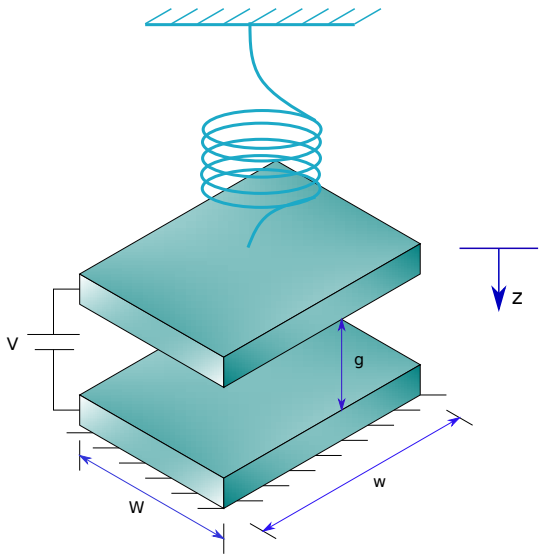

Figure 4.3: Lumped parallel-plate actuator system constrained by spring: electrostatic force pulls the upper plate downwards but mechanical spring force resits the movement.

$$m\ddot{z} + kz = F_e = \frac{\varepsilon_o A V^2}{2(g-z)^2} \tag{4.9}$$

where m is the mass of movable plate, k is the stiffness of spring (in our case k is the stiffness of beam as described previous chapter), A is the actuated area, ε_o is the dielectric constant of air, V is the applied potential DC voltage, g is the gap between the beam and the actuation electrode, z is the displacement of the cantilever beam due to the applied potential V.

There are tow ways to apply the electrostatic actuation potential between the cantilever beam and the electrode (i) DC actuation and (ii) AC actuation. If the structural instability phenomenon known as pull-in occurs due to only applied DC potential then it is called static pull-in and if both DC and AC actuation components cause structural instability then it is called dynamic pull-in [26]. In cantilever beam MEMS switches, an DC potential is applied whereas in resonator applications, both DC and AC actuation are applied. Now considering static pull-in, following equation is formed

$$kz = F_e = \frac{\varepsilon_o A V^2}{2(g-z)^2}. \tag{4.10}$$

The above equation is a cubic equation in z having three possible solutions. One solution can be $z > g$ which is non-physical and abandoned. Another solution represents

the equilibrium position $z = g$ which is unstable condition. Therefore, the only solution is left in response of DC actuation voltage which holds the stable solution of system and that is $z < g$. Again, if the equation (4.10) is written as

$$V = \sqrt{\frac{2kz}{\varepsilon_o A}}(g - z) \tag{4.11}$$

and plot the the gap versus applied voltage, two possible beam positions for every applied voltage would be found.

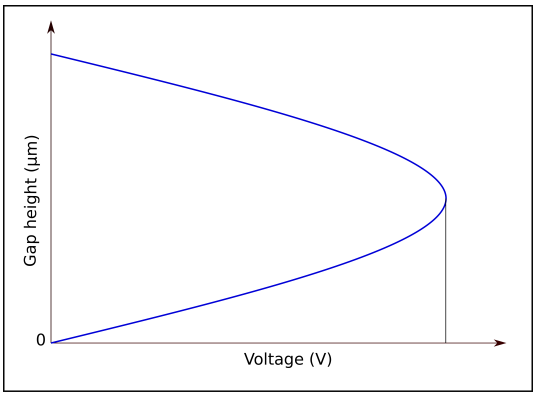

Figure 4.4: Two possible beam positions for every applied voltage.

Now to find the pull-in voltage associated with pull-in phenomenon, derivative of equation (4.11) with respect to z is conducted and set equal to zero

$$\frac{\partial V}{\partial z} = \sqrt{\frac{k}{2\varepsilon_o A z}}(g - z) - \sqrt{\frac{2kz}{\varepsilon_o A}} = 0. \tag{4.12}$$

After accomplishing simple mathematical calculation, following relation is found

$$z = \frac{1}{3}g. \tag{4.13}$$

So, at $z = \frac{1}{3}g$ structural instability occurs and at this position of the cantilever beam, pull-in voltage is evaluated. Now substitution this value in equation (4.11) leads to

$$V_{PI} = \sqrt{\frac{8kg^3}{27\varepsilon_o A}}. \tag{4.14}$$

Above equation is the well known pull-in voltage equation.

4.4 Switching Time

Switching time is defined as the time which is required for getting the first contact between the cantilever beam and the ground output electrode. Switching time is also called switch opening time. During actuation phenomenon, when applied potential surpasses pull-in voltage, structural instability occurs, static equilibrium no more exists and hence dynamic behavior must be taken into account to analyze the cantilever beam switches [27].

4.4.1 Squeeze Film Damping

In MEMS applications, squeeze film damping is a dominant phenomenon since dimensions of MEMS structures are at macro level. When a volume of fluid (gas or air) is displaced or squeezed due to the motion of its surrounded surfaces that causes an energy dissipation effect. This energy dissipation effect acts as damping force to resist the motion of moving surfaces. This phenomenon is called squeeze film damping. In MEMS switches, when gap between moving switch and fixed electrode is contracted due to the motion of switch towards the ground electrode, squeeze film damping effect exerts pressure on the surface of the switch to resist the motion of the moving switch. The distribution of this gas pressure is governed by the following non-linear Reynolds equation [28]

$$\frac{\partial}{\partial x}(\frac{Ph^3}{\mu}\frac{\partial P}{\partial x})+\frac{\partial}{\partial y}(\frac{Ph^3}{\mu}\frac{\partial P}{\partial y})=12\frac{\partial hP}{\partial t} \tag{4.15}$$

where P is the pressure in the gas film, and it is defined as $P = P_a + \Delta P$ where P_a is the ambient pressure and ΔP is the deviatory pressure, μ is the coefficient of viscosity, h is the thickness of the film which is defined as $h = h_0 + \Delta h$ where h_o is the initial thickness of film. Since MEMS switches have small oscillation amplitude and the gap between the switch and the fixed electrode is very small, hence pressure change is also small in the gas film ($\Delta h \ll h_0$ and $\Delta P \ll P_a$). Then a linearized form of the non-linearized Reynolds equation can be obtained as following

$$\frac{P_a h_0}{\mu}\left(\frac{\partial^2 P}{\partial x^2}+\frac{\partial^2 P}{\partial y^2}\right)=12\frac{\partial(hP)}{\partial t} \tag{4.16}$$

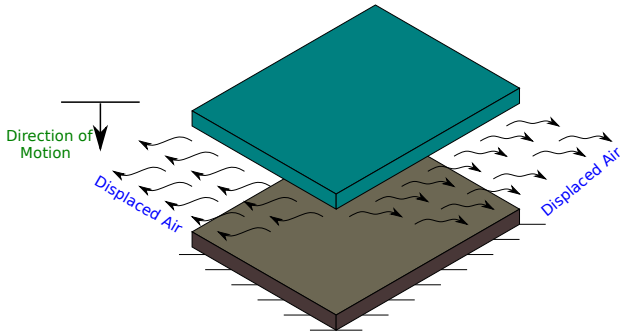

Figure 4.5: Illustration of squeezed-film damping: air has been displaced due to the downwards movement of upper plate.

$$\frac{\partial^2 P}{\partial x^2}+\frac{\partial^2 P}{\partial y^2}=\frac{12\mu}{h_0^3}\frac{\partial P}{\partial t}+\frac{12\mu}{h_0^2 P_a}\frac{\partial h}{\partial t}. \tag{4.17}$$

At small pressure, the mean free path of gas molecular λ is not negligible compared to film thickness. The mean free path is given by the following empirical equation

$$\lambda=\frac{1}{\sqrt{2\pi}N\sigma^2} \tag{4.18}$$

where σ is diameter of gas molecule and N is the number of molecule. The viscosity of gas is measured by Knudsen number which is given by

$$K_n=\frac{\lambda}{h_0}. \tag{4.19}$$

Viscosity changes with this Knudsen number, hence concept of effective viscosity is introduced. A well known empirical relation between effective viscosity and Knudsen number was derived by Veijola *et al.* [29] as follows:

$$\mu_{eff}=\frac{\mu}{1+9.638K_n^{1.159}}. \tag{4.20}$$

In order to evaluate the squeeze film damping force on switch surface, the exerted force on switch surface area at every moment is required to be determined during actuation. The dynamic governing equation of the system is written as

$$EI\frac{\partial^4 w}{\partial z^4}+\rho A\frac{\partial^2 w}{\partial t^2}+c\frac{\partial w}{\partial t}=F_e. \tag{4.21}$$

In order to analyze the static and dynamic behavior of any system, finite element method is widely used due to several advantages. The main advantages of this method are that it can handle very large number of degree of freedom, it can analyze stresses distribution through a complicated geometry and multi-physical effects in structure such as structural, electrical, fluidic, magnetic effect etc [30]. Now discretization of equation (4.21) by finite element method leads to

$$[M][\ddot{w}] + [C][\dot{w}] + [K][w] = [F_e] \tag{4.22}$$

where M is the mass, C is the damping, K is the stiffness matrices of the system. The solution of the above equation can be written as a linear combination of normal modes or eigenvectors, ϕ_j and generalized coordinates, η_j where j goes for 1 to N and N is the total number of normal mode [31]. From the modal matrix concept, It is known that if N number of normal modes can be assembled in a square matrix P then P is called the modal matrix. Then applying coordinate transformation, displacement z can be written as $P\eta$. Now considering the orthogonal property of eigenvectors and pre-multiplication of equation (4.22) by transpose of P or P^T leads to

$$P^T MP\ddot{\eta} + P^T CP\dot{\eta} + P^T KP\eta = P^T F_e \tag{4.23}$$

where $P^T MP$ and $P^T KP$ are orthogonal matrices due to orthogonal property. Now for $P^T CP$ to be a orthogonal matrix, damping matrix C has to be proportional to mass matrix, M or stiffness matrix, K or their linear combination i.e $C = \alpha M + \beta K$. This assumption of the damping matrix as a linear combination or proportion to the mass and the stiffness matries is knowa as Rayleigh damping. After applying Rayleigh damping, equation (4.23) will be completely uncoupled and its jth equation will have the following form [32]

$$\ddot{\eta}_j + 2\xi_j\omega_j\dot{\eta}_j + \omega_j^2\eta = \bar{F}_e. \tag{4.24}$$

Therefore, instead of N number of coupled equations, N number of uncoupled equations are obtained

$$\ddot{\eta}_N + 2\xi_N\omega_N\dot{\eta}_N + \omega_N^2\eta = \bar{F}_e \tag{4.25}$$

and

$$P^T CP = \begin{bmatrix} \alpha+\beta\omega_1 & 0 & . & . & 0 \\ 0 & \alpha+\beta\omega_2 & . & . & 0 \\ . & . & . & . & . \\ . & . & . & . & . \\ 0 & . & . & . & \alpha+\beta\omega_N \end{bmatrix}. \tag{4.26}$$

Now, on orthogonal transformation, following damping relations are obtained

$$2\xi_1\omega_1 = \alpha+\beta\omega_1$$

$$2\xi_2\omega_2 = \alpha+\beta\omega_2$$

.....

.....

$$2\xi_N\omega_N = \alpha+\beta\omega_N. \tag{4.27}$$

It has been shown in [33] that for only first 15 modes of most large engineering systems, mass has significant contribution. In MEMS technology, it is assumed that most MEMS actuation devicees are fabricated to function below first resonance frequency i.e MEMS switches or at first resonance frequency i.e. accelerators, gyroscopes, resonators [34]. Based on this assumption, it can be said that the maximum operating frequency of MEMS actuation devices is first resonance frequency. Therefore, there is no need to satisfy Rayleigh damping relation for more than first resonance frequency

$$2\xi_1\omega_1 = \alpha+\beta\omega_1. \tag{4.28}$$

Since there is two unknown parameters in one equation then the second resonance frequency is needed to get the solution

$$2\xi_1\omega_2 = \alpha+\beta\omega_2. \tag{4.29}$$

Solving equation (4.28) and equation (4.29), following relations are obtained

$$\alpha = 2\omega_1\omega_2\frac{(\xi_1\omega_2-\xi_2\omega_1)}{\omega_2^2-\omega_1^2} \tag{4.30}$$

and

$$\beta = 2\frac{(\xi_2\omega_2-\xi_1\omega_1)}{\omega_2^2-\omega_1^2} \tag{4.31}$$

where, the damping co-efficient ξ_1 and ξ_2 are calculated by

$$\xi_1 = \frac{c_{resonance,1}}{c_{crit,1}}; c_{crit,1} = 2m_1\omega_1 \tag{4.32}$$

and

$$\xi_2 = \frac{c_{resonance,2}}{c_{crit,2}}; c_{crit,2} = 2m_2\omega_2. \tag{4.33}$$

Terms ω_1, ω_2, m_1, m_2 can be determined in CoventorWare from a MemMech modal analysis. Then critical damping $c_{crit,1}$ and $c_{crit,2}$ are computed using equation (4.32) and equation (4.33). Damping co-efficient at resonance frequencies $c_{resonance,1}$ and $c_{resonance,2}$ can be determined in CoventorWare from a DampingMM /mode shape analysis. Then ξ_1, ξ_2, α and β are determined from above equations using ω_1, ω_2, m_1, m_2, ξ_2 and ξ_2.

4.5 Contact Force

The reliability and longevity of MEMS contact switches greatly depend on the contact between electrodes. The contact phenomenon between electrodes in MEMS switches usually is a very complicated analysis due to the presence of multi-physical effects such as mechanical, electrical, chemical, thermal etc. Several parameters are linked to contact phenomenon among them contact resistance, contact area and contact force are most important which ensure the reliable function and longevity of MEMS contact switches. Contact resistance has to be low as much as possible to prevent the heat generation due to joule heating effect governed by I^2R_ct wehere I is current flow, R_c is the contact resistance and t is the time. Because suffiecient heat can soften or annel the contact region resuling in stiction or adhesion problem. Holm [7] has given an expression for contact resistance considering the circular contact spot having contact radius a

$$R_c = \frac{\rho_1 + \rho_2}{4a} \tag{4.34}$$

where ρ_1 and ρ_2 resistivities of contact materials. In the case of similar contact material the expression becomes

$$R_c = \frac{\rho}{2a}. \tag{4.35}$$

Contact force and contact area play significant roles to reduce contact resistance. High contact force ensures large effective contact area which results in low contact resistance. Increase in contact forces resulting in low the contact resistance has been reported in studies [35, 36, 37]. Contact phenomenon in MEMS switches is a non-linear problem where the cantilever beam approaches the rigid contact electrode and after reaching contact point it can not go further. If application of force is being continued then cantilever beam gets deformed by the rigid electrode. The cantilever beam is called salve surface and the rigid electrode is called master surface. Considering the deformation of contact materials, following revised contact resistance equation was proposed in [38]

$$R_c = 0.886\rho\sqrt{\frac{H}{F_c}} \tag{4.36}$$

where ρ resistivity of contact material, H is the hardness of contact material and F_c contact force.

In order to evaluate contact force between electrodes at the downstate position, the system has been considered as a fixed-simply supported beam phenomenon. Now let us consider the following Figure 4.6 which depicts the downstate contact position of beam.

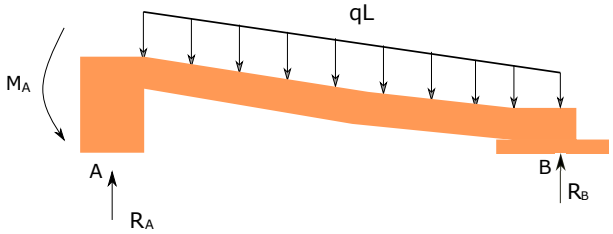

Figure 4.6: Fixed-simply supported model of MEMS switch.

There will be two reaction forces; one is at the fixed end, R_A and another one is at the simply supported end, R_B and a moment at the fixed end, M_A. Now considering free body diagram, following equation can be written

$$+\uparrow \sum F_y = 0 : R_A + R_B - qL = 0. \tag{4.37}$$

And considering upward concave bending positive

$$\sum M_A = 0 : M_A + R_B L - \frac{1}{2}qL^2 = 0. \tag{4.38}$$

Now considering free body diagram of a portion *AC* of beam, following equation can be written

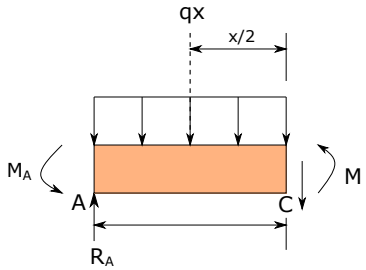

Figure 4.7: Free body diagram of a portion of the beam

$$EI\frac{d^2y}{d^2x} = -\frac{qx^2}{2} + R_A x - M_A. \tag{4.39}$$

Integrating twice in x,

$$EIy = -\frac{qx^4}{24} + \frac{R_A x^3}{6} - \frac{M_A x^2}{2} + C_1 x + C_2. \tag{4.40}$$

Now applying the boundary condition $x = 0$, $\frac{dy}{dx} = 0$ and $x = 0$, $y = 0$ in equation (4.40), equation (4.40) can be written as follows:

$$EIy = -\frac{qx^4}{24} + \frac{R_A x^3}{6} - \frac{M_A x^2}{2}. \tag{4.41}$$

Now applying another boundary condition $x = L$, $y = 0$ in equation (4.41) leads to

$$0 = -\frac{qL^4}{24} + \frac{R_A L^3}{6} - \frac{M_A L^2}{2}$$

$$3M_A - R_A L + \frac{qL^2}{4} = 0. \tag{4.42}$$

Now solving equation (4.37), equation (4.38)and equation (4.43) simultaneously, the reaction forces and moment at the supports are obtained as follows:

$$R_A = \frac{5}{8}qL, M_A = \frac{1}{2}qL^2, R_B = \frac{3}{8}qL$$

. Therefore, the reaction force at contact point is

$$F_c = \frac{3}{8}qL = \frac{3}{8} \times F_t \tag{4.43}$$

where F_t is total distributed load. In MEMS switches operation, when a DC voltage is applied between the cantilever beam and the ground electrode, an electrostatic force is induced. This electrostatic force pulls the beam downwards the ground electrode. A restoring mechanical force will resist the electrostatic actuation force. Therefore, in order to pull down the beam, electrostatic force is to overcome this mechanical restoring force. Therefore, the total contributing force on the beam at downstate position can be written as

$$F_t = qL - \Delta g K_r. \tag{4.44}$$

where Δg is the beam tip displacement and K_r is the restoring beam stiffness. The restoring stiffness of beam at downstate position is equivalent to $\frac{3EI}{L^3}$ [16]. Therefore, the actual contact force can be approximated as

$$F_c = \frac{3}{8}(qL - \Delta g K_r). \tag{4.45}$$

In MEMS contact switches application, qL is the transverse electrostatic force which is uniformly distributed over the actuation area of the beam. At downstate position this force is evaluated from equation (4.8).

CHAPTER 5

MECHANICAL DESIGN AND FORMULATION OF RESULTS

The Figure 5.1, Figure 5.2 and Figure 5.3 depict simplified structure of MEMS contact switch to be analyzed. The cantilever beam with length L, width W and thickness t has been suspended at height g_o above the pull-down electrode. The pull-down electrode has been placed at a distance d from the anchor point. A DC voltage V is applied during operation of MEMS switch. This DC voltage induces a transverse electrostatic force which is uniformly distributed over the actuation area of the beam Wl that causes deflection of the beam. Fringing electric fields have been neglected since the gap between actuation electrode and the cantilever beam is small compared with the length of cantilever beam. A rectangular dimple has been patterned at the free end of the beam to close the contact gap before the portion of beam above actuation electrode makes any contact with the actuation electrode and shorts the system. Dimple has 2 μm width and 0.2 μm height. A contact electrode has been placed underneath the dimple for signal transmission. The mechanical design of electrostatic based MEMS switches greatly depends on applied voltage. The well known pull-in voltage equation, which has been formulated at previous chapter, is

$$V_{PI} = \sqrt{\frac{8k(g_o)^3}{27\varepsilon A}}.$$

This well known formula implies that a number of ways are available to reduce the pull-in voltage. For example, lowering g_o can considerably reduce pull-in voltage. But this creates a trade-off with isolation and insertion loss of switch because low gap provides large actuation force with low applied voltage but causes intolerable isolation and insertion loss. To solve this trade-off, gap g_o has been fixed carefully as 0.5 μm. Another step to lower the pull-in voltage is to make large the actuation area. A third step is to reduce the stiffness of beam which requires higher length.

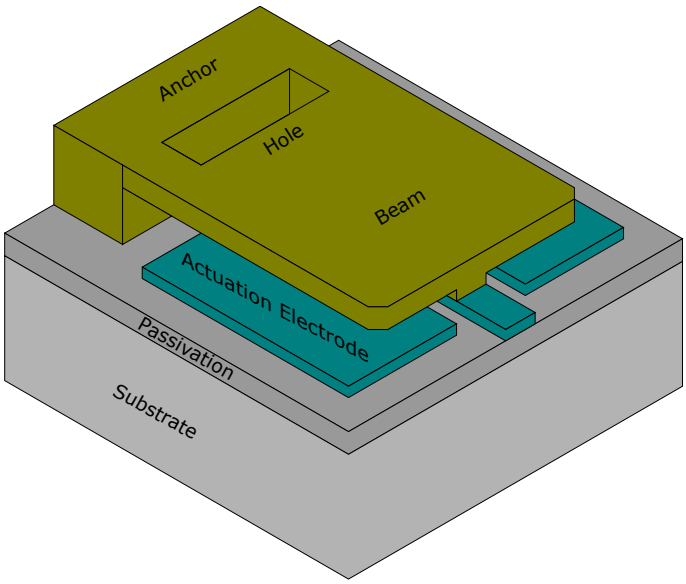

Figure 5.1: 3D schematic view of simplified model of MEMS cantilever beam switch.

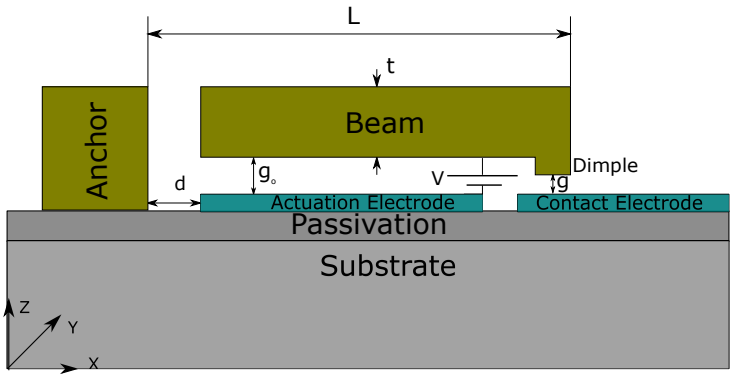

Figure 5.2: Cross-section view of simplified model of MEMS cantilever beam switch.

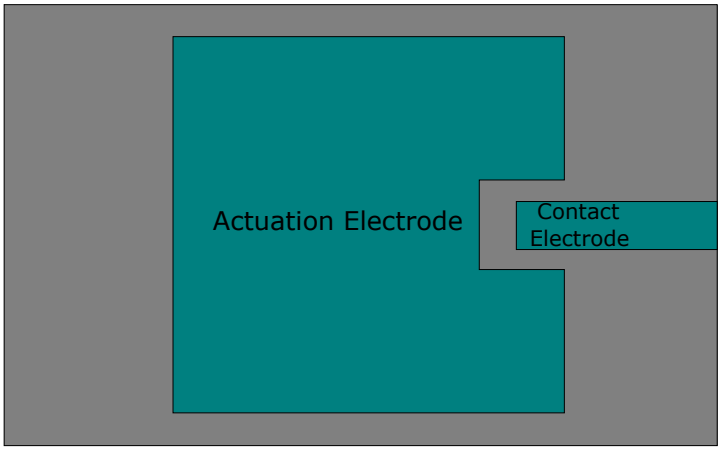

Figure 5.3: Top view of simplified model of MEMS cantilever beam switch without cantilever beam.

Both these two ways increase size and mass of switch and it violates purpose of miniaturization. Moreover, increase of mass also increases the switching time. To solve these trade-off, it has been suggested in [17] that small width at the anchor point significantly decreases stiffness of the beam resulting in low pull-in voltage. Following this research corollary, a rectangular hole has been introduced at the anchor point which ensures low stiffness, low mass, size limitation, low switching time and low pull-in voltage. Moreover, this rectangular hole also reduces the squeeze film damping effect on beam which further reduces switching time. In order to ensure large actuation area, length of rectangular hole has been fixed as d so that the area of beam over pull-down electrode is not reduced. For smooth signal transmission, moderate contact force is essential which will ensure stable contact between electrodes but not too much high to create stiction problem. To ensure that moderate contact force, a moderate dimple contact area 2 $\mu m \times$ 2 μm has been considered. The corner edges of beam at front part have been removed to avoid stress concentration during manufucting. Beam, pull-down electrode and contact electrode are made of gold. The whole structure has been constructed on a silicon wafer but separated by a dielectric oxide layer. The mechanical properties of gold have been presented in Table 5.1. These properties have been used in different studies for satisfactory performance [14, 16, 39].

Table 5.1: Mechanical properties of different parts of beam.

Layer Name	Materials Name	$E(GPa)$	ν	ρ (Kg/m^3)	$R\ (\Omega)$	$H\ (Gpa)$
Beam	Gold	40	0.44	1.93e-14	2.04e-8	2
Actuation electrode	Gold	40	0.44	1.93e-14	2.04e-8	2
Contact electrode	Gold	40	0.44	1.93e-14	2.04e-8	2

E: young's modulus of gold, ν: passion's ratio, ρ: density of gold, R: resistivity of gold, H: hardness of gold.

In order to find out the optimized shape of MEMS contact switch, 4 cases have been considered based on the thickness of beam in where at each case, different beam

dimensions have been considered. Four cantilever beams with 1 μm , 1.2 μm, 1.4 μm and 1.6 μm thickness have been analyzed. Dimension of beam has been changed from $10\mu m \times 10\mu m$ to $30\mu m \times 30\mu m$ with an interval of $2\mu m \times 2\mu m$ which results in 11 configurations for each distinct beam. Table 5.2 and 5.3 show four beams with four different thickness and the Dimensions of 11 configurations of each of them.

Table 5.2: Four beams with distinct thickness.

Number of case	Thickness (μm)
1	1.6
2	1.4
3	1.2
4	1

Table 5.3: Dimensions of 11 configurations of each beam.

Configuration No.	Dimensions of beam ($l_s \times w_s$)	Dimensions of rectangular hole ($l_h \times w_h$)	Actuation area (μm^2)
1	$10 \times 10\mu m$	$4 \times 5\mu m$	35
2	$12 \times 12\mu m$	$4 \times 8\mu m$	71
3	$14 \times 14\mu m$	$4 \times 9\mu m$	115
4	$16 \times 16\mu m$	$4 \times 10\mu m$	158
5	$18 \times 18\mu m$	$4 \times 12\mu m$	218
6	$20 \times 20\mu m$	$4 \times 13\mu m$	286
7	$22 \times 22\mu m$	$4 \times 14\mu m$	362
8	$24 \times 24\mu m$	$4 \times 15\mu m$	446
9	$26 \times 26\mu m$	$4 \times 16\mu m$	538
10	$28 \times 28\mu m$	$4 \times 17\mu m$	638
11	$30 \times 30\mu m$	$4 \times 18\mu m$	746

l_s: length of switch, w_s: width of switch, l_h: length of hole, w_h: width of hole.

The performance characteristics parameter of MEMS switch, pull-in voltage, contact

force and switching time, have been obtained from simulation and analytically; and compared with literature. Switching time with squeeze film damping has been obtained and its effect on switching speed has also been analyzed. CoventorWare software, which is dedicated to MEMS designing and simulations, has been used to analyze MEMS switch. Simulations have been performed in CoventorWare to determine pull-in voltage, contact force and switching time. 3D finite element method extruded bricks mesh has been used to analyze switch in CoventoWare. Extruded bricks mesh is created by applying hexahedral mesh by the extrusion of surface in z-direction. Pull-in voltage has been determined in CoventroWare from CoSolveEM solver which uses 3D finite element method to solve coupled elector-mechanical problem. CoSolveEM solver applies DC bias voltage between the beam and the actuation electrode which induces electrostatic force between two parts. CoSolveEM increases the DC voltage until it find a divergent result for a specified voltage after a convergent solution for a specified voltage. Then CoSolveEM performs a bisection search to find the pull-in voltage.

Contact force simulations have been conducted in CosolveEM analysis of CoventorWare. Applied DC bias voltage between the beam and the actuation electrode induces electrostatic force which causes deflection of the beam. In simulation, the beam and the actuation electrode have been assigned as slave and master surface in contact pairs, respectively. Contact force has also been analytically calculated from equation (4.45). Using calculated contact force, contact resistance has been calculated from equation (4.36).

Switching time has been evaluated by conducting dynamic response analysis of beam in MemMech transient analysis of CoventorWare. To analyze damping effect on dynamic response, simulations have been conducted in MemMech transient analysis applying squeeze film damping. To estimate damping, damping co-efficient are calculated by modal shape analysis method. Modal analysis of beam has been conducted in MemMech modal analysis solver to find the natural frequencies and model shapes of the structure. The first six resonance mode shapes have been evaluated. Two resonance mode shapes from six mode shapes have been considered to compute damping parameters. Critical damping of mode shapes has been computed using $c_{crit} = 2m\omega$. In DampingMM solver of CoventorWare, damping co-efficient at resonance frequen-

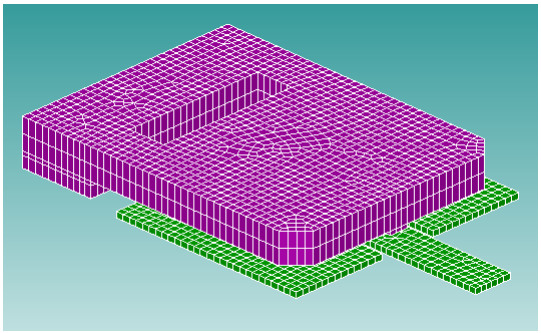

Figure 5.4: 3D view MEMS cantilever beam switch in CoventorWare with extruded bricks mesh.

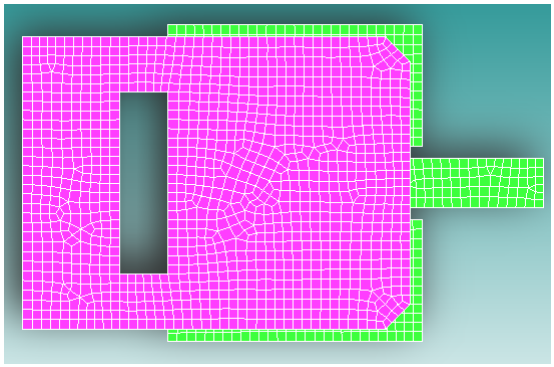

Figure 5.5: Top view MEMS cantilever beam switch in CoventorWare with extruded bricks mesh.

cies of six mode shapes have been computed. Then, damping co-efficient at resonant frequency of two mode shapes have been used to compute the modal damping ratio ξ by equation (4.32) and equation (4.32). To evaluate the damping effect on beam dynamics, Rayleigh damping has been considered as described at previous chapter. Damping matrix C, which is proportional to mass matrix M and stiffness matrix K, has been computed from $C = \alpha M + \beta K$. Constants α and β have been computed from equation (4.30) and equation (4.31), respectively. After that, constants α and β have been used as material damping boundary conditions in MemMech transient analysis solver of CoventorWare to determine switching time of beam under damping condition.

CHAPTER 6

RESULTS AND DISCUSSION

6.1 Case 1: Cantilever Beam with Thickness 1.6 μm

6.1.1 Pull-in Voltage (V_{PI})

To validate pull-in voltage results of beam with hole, at first CoventorWare model of beam without hole has been validated with analytic model. Analytically calculated pull-in voltage from equation (4.14) and 3D simulated pull-in voltages from CoventorWare have been shown in Table 6.1 and depicted in Figure 6.1. Mesh convergence analysis has been conducted to find pull-in voltages.

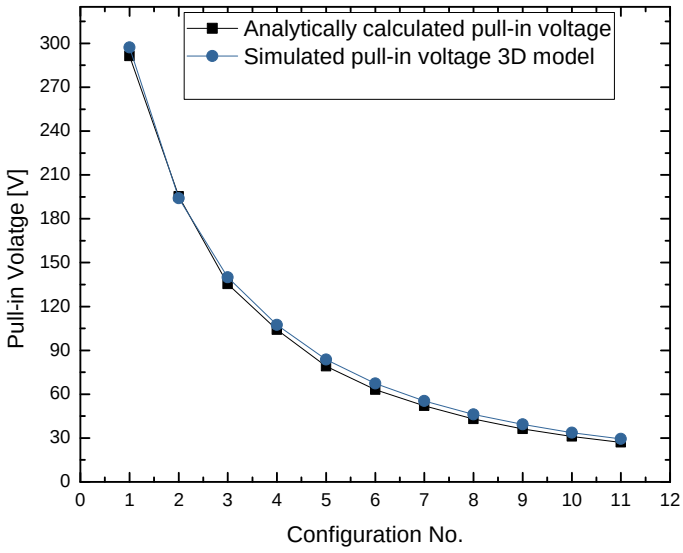

Figure 6.1: Comparison of pull-in voltage of 11 configurations between analytic model and 3D CoventorWare model.

Pull-in voltage results obtained from CoventorWare agree with pull-in voltage of analytic results. Pull-in voltage decreases with increase of dimension of the beam at both analytic and 3D model. This decrease is a direct effect of increase of the beam length which decreases the stiffness of beam. Since pull-in voltage is proportional to beam stiffness, decrease of stiffness has reduced pull-in voltage, and vice versa.

Table 6.1: Analytically calculated pull-in voltage and CoventorWare simulated pull-in voltage of 11 configurations of switch having no hole with thickness 1.6 μm.

Configuration No.	Analytically calculated pull-in voltage, (V)	CoventorWare simulated pull-in voltage,(V) 3D model
1	291.27	297.18
2	195.34	194.06
3	135.38	140
4	104.17	107.5
5	79	83.75
6	63	67.18
7	52	55.31
8	43	46.25
9	36.26	39.37
10	31.12	33.75
11	27.01	29.37

It is important to conduct a mesh convergence study to verify that a sufficiently refined mesh has been applied to model switch accurately. Refined mesh ensures accurate result. The numerical solution provided by model will tend towards a unique value as the mesh density is increased. The mesh is said to be converged when further mesh refinement produces a negligible change in the solution. When the two meshes give identically the same result then it means that model is producing mathematically accurate solution .

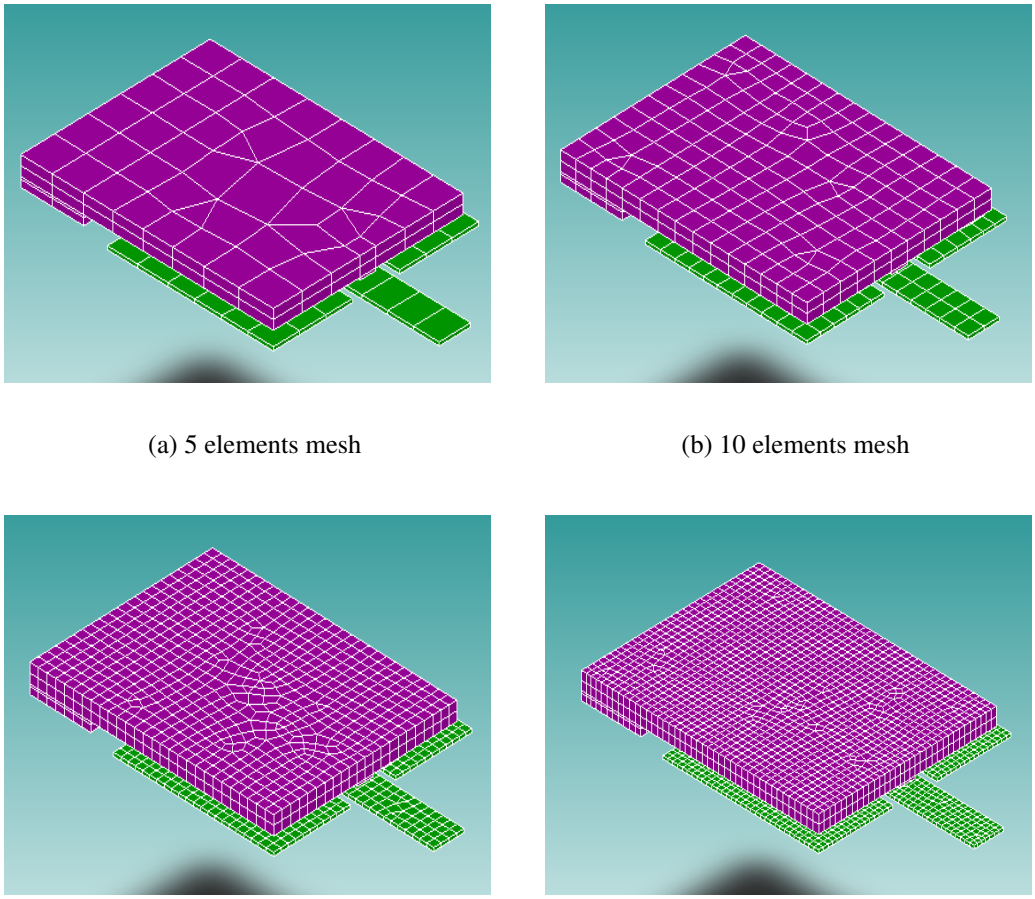

(a) 5 elements mesh

(b) 10 elements mesh

(c) 20 elements mesh

(d) 30 elements mesh

Figure 6.2: Mesh convergence analysis of configuration 8.

To verify the accuracy in pull-in voltages produced by 3D CoventorWare model, mesh convergence study of configuration 8, dimension $24 \times 24 \mu m$, has been conducted. Results for different element size have been depicted in Figure 6.3. It is seen from figure that increase of element number gives more accurate pull-in voltage. Pull-in voltage has been found as 48.12 V, 47.5 V, 46.56 V and 46.25 V for element 5, 10, 20, 30, respectively. After 30 element, increase of element number does not effect pull-in voltage. Element number of 30, 40 and 50 give same pull-in voltage as 46.25 V. It means that mesh has been converged. Therefore, it can be said that 3D CoventorWare model has produced mathematically accurate solution.

Now following the same procedures, pull-in voltages of 3D CoventorWare model with hole have been determined.

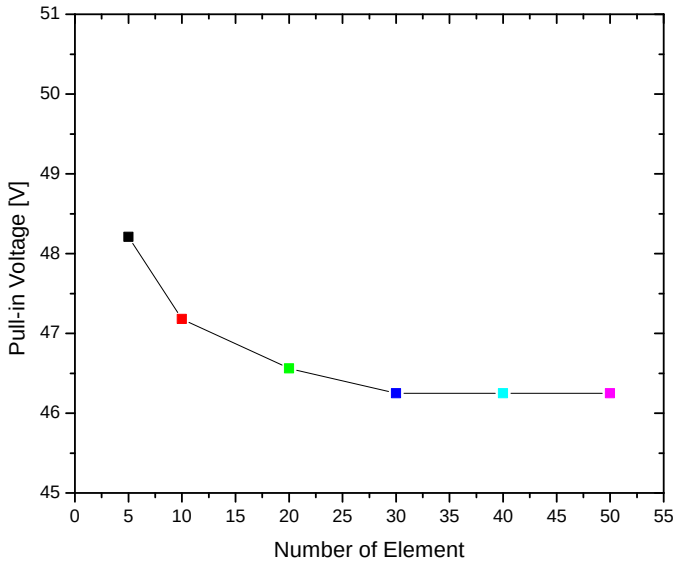

Figure 6.3: Mesh convergence analysis of pull-in voltage results of configuration 8.

Table 6.2: CoventorWare simulated pull-in voltage of 11 configurations of switch having hole with thickness 1.6 μm.

Configuration No.	CoventorWare simulated pull-in voltage,(V) 3D model
1	225
2	118.13
3	86.88
4	70.62
5	51.56
6	42.50
7	35.62
8	30.31
9	26.25
10	22.81
11	20.31

Table 6.2 shows pull-in voltage results of 3D CoventorWare model with hole. It is seen that pull-in voltage decreases significantly due to hole at the anchor point. Introduction of hole at anchor point has significantly decreased stiffness of beam. It is because introduction of hole at anchor point reduces the inertia effect of beam during bending which in turn reduces the stiffness of beam. Since pull-in voltage is proportional to beam stiffness, decrease of stiffness decreases pull-in voltage, and vice versa. Thus pull-in voltage has been reduced after introducing of hole. Regarding dimension change effect, it shows the same trend as no hole case. Pull-in voltage decreases with increase of dimension due to reduction in stiffness.

6.1.2 Switching Time

Simulated damped and undamped switching time of MEMS switches with hole having thickness 1.6 μm have been shown in Table 6.3. From switching time results, it is seen that switching time becomes smaller with decrease of dimension.

Table 6.3: Undamped and damped switching time of 11 configurations of switch with hole having thickness 1.6 μm.

Configuration No.	Switching time at $1.5V_{PI}$ without damping (μs)	Switching time at $1.5V_{PI}$ with damping (μs)
1	0.15	0.15
2	0.296	0.296
3	0.297	0.297
4	0.43	0.45
5	0.54	0.58
6	0.59	0.60
7	0.74	0.75
8	0.90	0.91
9	1.02	1.04
10	1.05	1.08
11	1.17	1.33

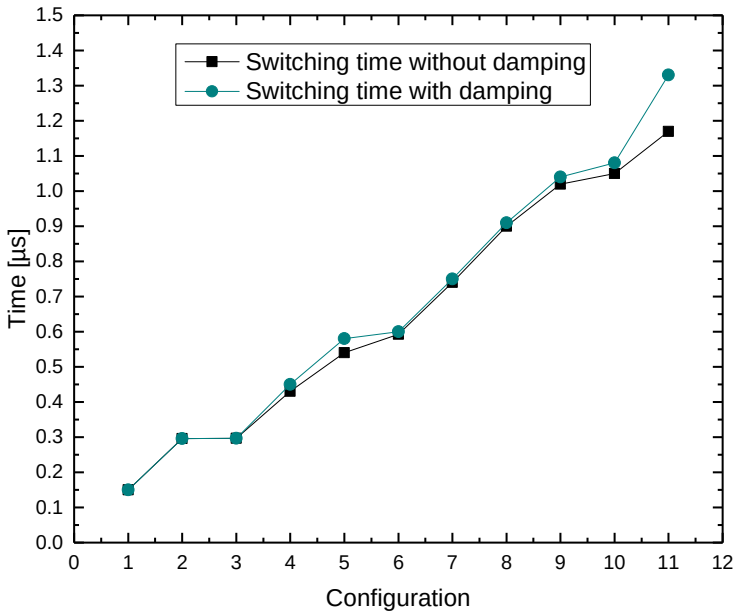

Figure 6.4: Damped and undamped switching time of 11 configurations of switch with thickness 1.6 μm.

This decrease of switching time is the consequence of increase of pull-in voltage. Higher pull-in voltage ensures lower switching time. Switching time strongly relies on pull-in voltage because large pull-in voltage ensures high actuation force which in turn increases switch speed. It is seen that damping effect on switching time is significant for large dimension switch. But damped switching time is very similar to the undamped switching time in case of small dimension switch. Configurations from 1 to 3 give same switching time for damped and undamped condition. In contrast, switching time of configuration from 4 to 11 under damped condition are higher than undamped condition. This can be attributed to high actuation force because of high pull-in voltage of small dimension switch. Because as actuation force gets larger, damping force exerts less influence on dynamic behavior.

The response of undamped and damped condition of four configurations have been shown in Figure 6.5. It is clear from figure that amplitude of response of under damped switch decreases with time.

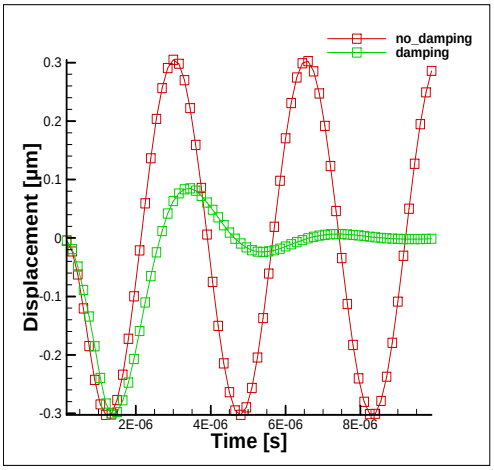

(a) Dimension 30×30

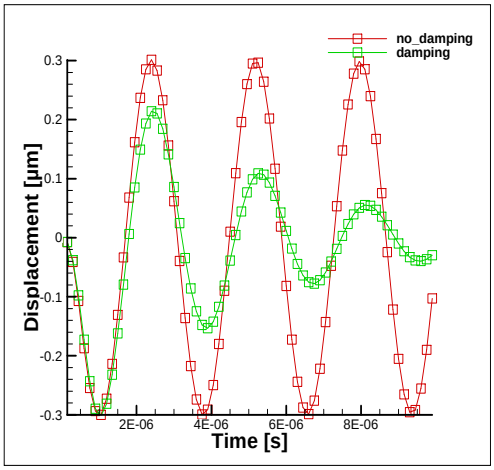

(b) Dimension 26×26

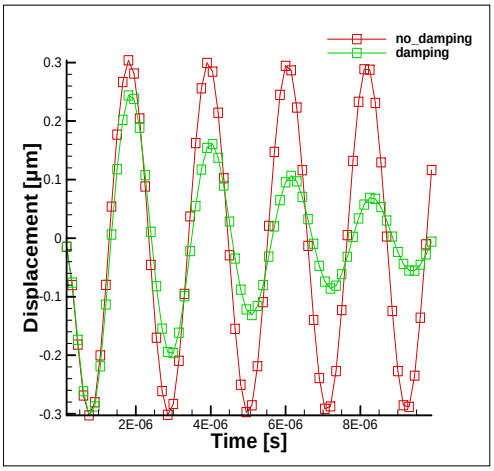

(c) Dimension 22×22

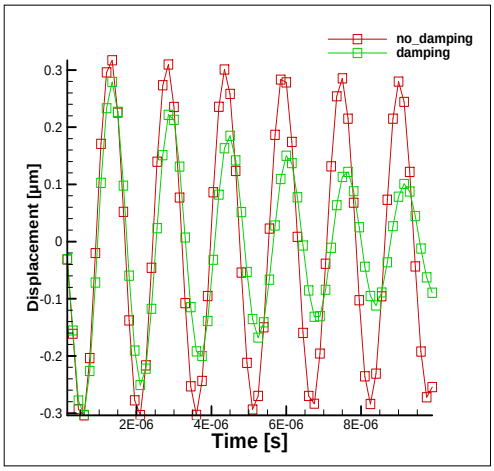

(d) Dimension 18×18

Figure 6.5: Comparison of damping with no damping of four configurations of switch with thickness 1.6 μm.

Under damped condition, the tip of switch makes only one contact with the transmission pad or contact electrode during first cycle. From second cycle, amplitude starts to decrease. Squeeze film damping causes amplitude reduction but frequency of switch remains same.

6.1.3 Contact Force

Actuation force, analytically calculated contact force, simulated contact force and contact resistance of 11 configurations of MEMS switch with thickness $1.6\mu m$ at applied voltage of 1.5 V_{PI} have been shown in Table 6.4. Actuation force and contact force have been determined at $1.5V_{PI}$ in order to get stable contact. Table 6.4 shows that simulated contact force for each configuration is consistent with analytically calculated contact force. Contact resistance decreases with increase of contact force which agrees with other research results [40, 41]. Rest of actuation force contributes to reaction force at the anchor and to overcome mechanical restoring force. Contact force has decreased with increase of dimension.

Table 6.4: Actuation force, analytically calculated contact force, CoventorWare simulated contact force and contact resistance of 11 configurations of switch with thickness 1.6 μm.

Configuration No.	Actuation force (μN) at $1.5V_{PI}$	Analytically calculated contact force (μN) at $1.5V_{PI}$	CoventorWare simulated contact force (μN) at $1.5V_{PI}$	Contact resistance (Ω)
1	293.44	86.99	82.33	0.086
2	145.96	44.07	44.79	0.122
3	121.02	36.99	36.27	0.139
4	101.18	31.19	29.02	0.144
5	73.27	22.73	22.81	0.169
6	63.86	19.91	20.51	0.181
7	55.94	17.51	17.87	0.192
8	49.28	15.48	16.33	0.21
9	43.68	13.76	14.67	0.22
10	38.93	12.29	13.58	0.23
11	34.89	11.03	12.56	0.24

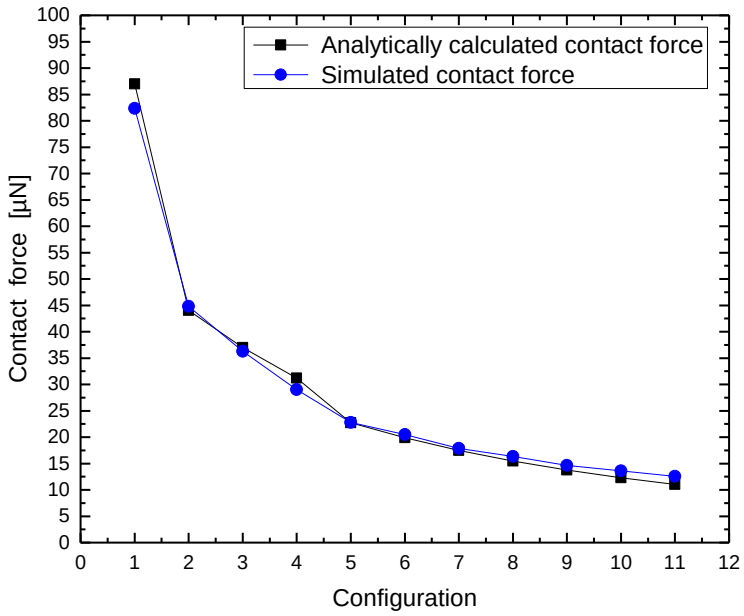

Figure 6.6: Analytic and simulated contact force of 11 configurations of switch with thickness 1.6 μm.

It has been reported in [23] that contact force is around 30-60% of actuation or pull-down force. In this study, for each configuration, contact force is in between 30-60% of actuation or pull-down force in both analytic and simulated results. Large dimension decreases pull-in voltage. Since contact forces have been determined at 1.5 times of pull-in voltage, thus contact force has been decreased.

6.2 Case 2: Cantilever Beam with Thickness 1.4 μm

6.2.1 Pull-in Voltage(V_{PI})

3D simulated pull-in voltage of 11 configurations of switch with hole having thickness 1.4 μm have been shown in Table 6.5. Compared with case 1, pull-in voltage decreases in each configuration. This decrease is direct effect of reduction in thickness of beam. Stiffness of beam is proportional to thickness of beam. Reduction of thickness decreases stiffness of beam. Again pull-in voltage is proportional to beam stiffness. As a results, reduction of thickness has reduced pull-in voltage.

Table 6.5: CoventorWare simulated pull-in voltage of 11 configurations of switch with hole having thickness 1.4 μm.

Configuration No.	CoventorWare simulated pull-in voltage, (V) 3D model
1	188.43
2	99.06
3	72.50
4	58.75
5	42.81
6	35.31
7	29.69
8	25.31
9	21.87
10	19.06
11	16.56

6.2.2 Switching Time

Simulated damped and undamped switching time of MEMS switches with hole having thickness 1.4 μm have been shown in Table 6.6. In the case of switch with thickness 1.4 μm, switching time shows the very same trend as case 1. From switching time results, it is seen that switching time becomes smaller with decrease of dimension. Damped switching time is very similar to the undamped switching time in case of small dimension but for large dimension, discrepancy between undamped and damped switching time is noticeable. Configurations from 1 to 4 give same switching time for damped and undamped condition but configurations from 4 to 11 give remarkable difference between damped and undamped condition. This can be attributed to low actuation force because of low pull-in voltage of large dimension. Because as actuation force gets smaller, damping force exerts more influence on dynamic behavior. The response of undamped and damped condition of four configurations have been shown in Figure 6.7.

Table 6.6: Undamped and damped switching time of 11 configurations of switch with thickness 1.4 μm.

Configuration No.	Switching time at $1.5V_{PI}$ without damping (μs)	Switching time at $1.5V_{PI}$ with damping (μs)
1	0.153	0.153
2	0.3	0.33
3	0.421	0.433
4	0.444	0.444
5	0.59	0.591
6	0.69	0.744
7	0.74	0.845
8	0.88	0.97
9	1.027	1.049
10	1.15	1.16
11	1.18	1.32

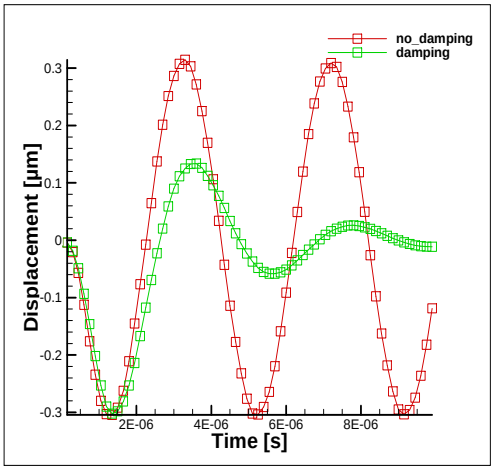

(a) Dimension 30×30

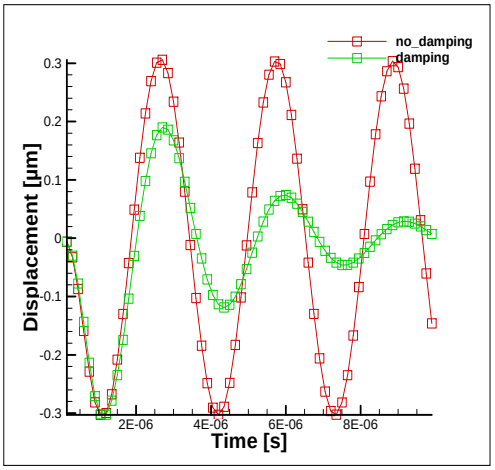

(b) Dimension 26×26

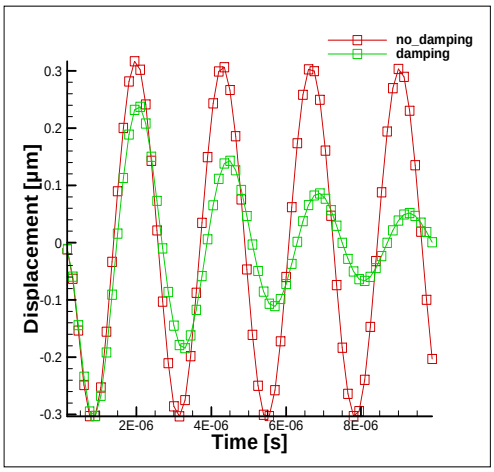

(c) Dimension 22×22

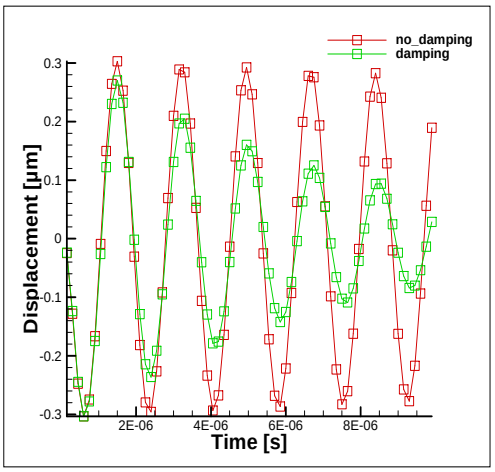

(d) Dimension 18×18

Figure 6.7: Comparison of damping with no damping of four configurations of switch with thickness 1.4 μm.

It is clear from figure that amplitude of response of under damped switch decreases with time. Under damped condition, the tip of switch makes only one contact with transmission pad or contact electrode during first cycle. From second cycle, amplitude starts to decrease. Squeeze film damping causes amplitude reduction but frequency of switch remains same.

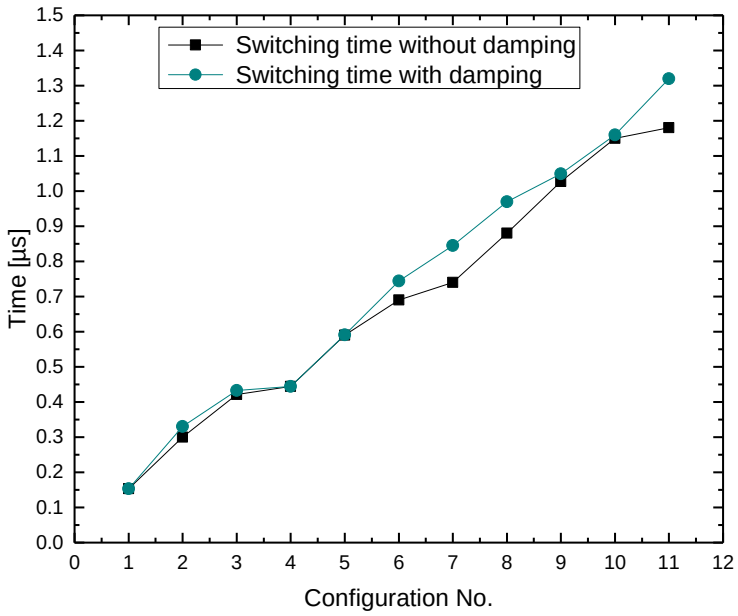

Figure 6.8: Damped and undamped switching time of 11 configurations of switch with thickness 1.4 μm.

6.2.3 Contact Force

Actuation force, analytically calculated contact force, simulated contact force and contact resistance of 11 configurations of MEMS switch with thickness 1.4 μm at applied voltage of 1.5 V_{PI} have been shown in Table 6.7. Actuation force and contact force have been determined at $1.5V_{PI}$ in order to get stable contact.

From contact force results of thickness 1.4 μm, it is clear that simulated contact force for each configuration agrees with analytically calculated contact force. For each configuration, contact force is around 30-60% of actuation or pull-down force. Compared with thickness 1.6 μm, contact force has decreased for each configuration. This decrease can be explained by attributing thickness reduction. Thickness reduction has decreased pull-in voltage which results reduction in applied voltage of $1.5V_p$. As a result, smaller actuation force has been generated than case 1. Contact resistance has been decreased with increase of contact force as predicted by equation (4.36). Compared with case 1, contact resistance has been reduced due to low contact force.

Table 6.7: Actuation force, analytically calculated contact force, CoventorWare simulated contact force and contact resistance at 1.5 V_{PI} of 11 configurations of switch with thickness 1.4 μm.

Configuration No.	Actuation force (μN) at $1.5V_{PI}$	Analytically calculated contact force (μN) at $1.5V_{PI}$	CoventorWare simulated contact force (μN) at $1.5V_{PI}$	Contact resistance (Ω)
1	156.98	58.28	61.67	0.106
2	97.78	29.52	28.52	0.149
3	81.07	24.78	25.64	0.163
4	67.78	20.89	20.10	0.177
5	49.08	15.23	15.60	0.207
6	42.78	13.44	13.97	0.221
7	37.47	11.73	12.57	0.236
8	33.01	10.37	11.51	0.251
9	29.26	9.22	10.89	0.266
10	26.06	8.23	9.36	0.282
11	23.33	7.39	9.21	0.297

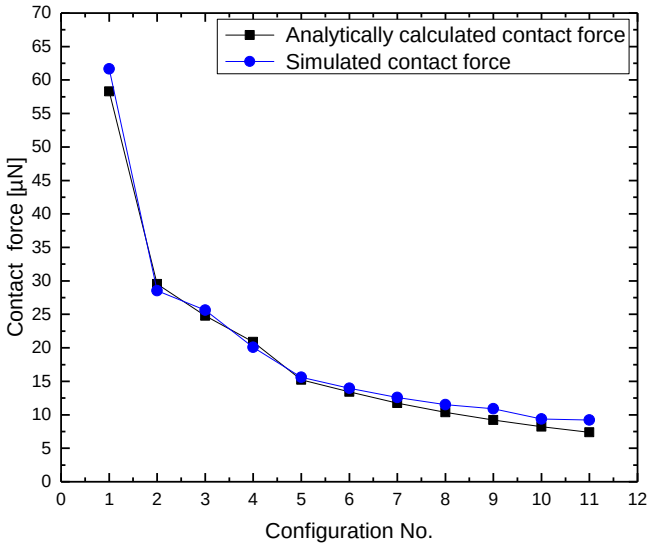

Figure 6.9: Analytic and simulated contact force of 11 configurations of switch with thickness 1.4 μm.

6.3 Case 3: Cantilever Beam with Thickness 1.2 μm

6.3.1 Pull-in Voltage(V_{PI})

3D CoventorWare simulated pull-in voltage of 11 configurations of switch with hole having thickness 1.2 μm have been shown in Table 6.8. Compared with case 1 and case 2, pull-in voltage decreases in each configuration. This decrease is direct effect of reduction in thickness of beam.

Table 6.8: CoventorWare simulated pull-in voltage of 11 configurations of switch with hole having thickness 1.2 μm.

Configuration No.	CoventorWare simulated pull-in voltage, (V) 3D model
1	153.12
2	80.31
3	58.44
4	47.50
5	34.69
6	28.44
7	23.75
8	20.31
9	17.50
10	15.31
11	13.44

6.3.2 Switching Time

Simulated damped and undamped switching time of MEMS switches with hole having thickness 1.2 μm have been shown in Table 6.9.

Table 6.9: Damped and undamped switching time of 11 configurations of switch with thickness 1.2 μm.

Configuration No.	Switching time at $1.5V_{PI}$ without damping (μs)	Switching time at $1.5V_{PI}$ with damping (μs)
1	0.154	0.154
2	0.3	0.3
3	0.44	0.44
4	0.45	0.45
5	0.6	0.69
6	0.75	0.83
7	0.84	0.9
8	1.04	1.05
9	1.17	1.182
10	1.34	1.36
11	1.46	1.62

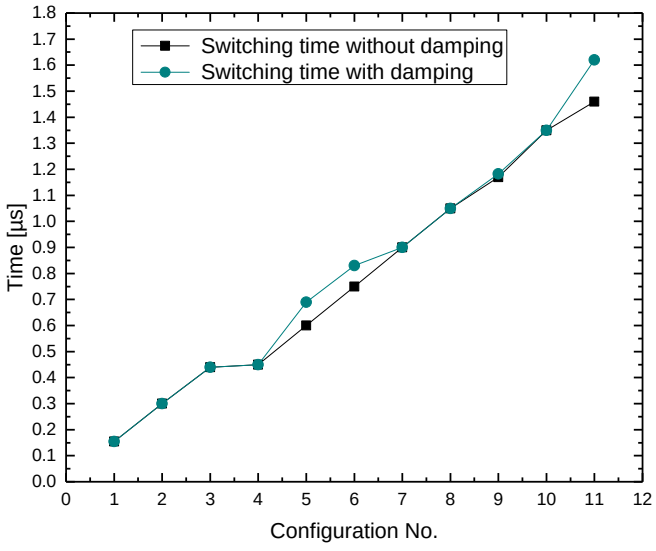

Figure 6.10: Damped and undamped switching time of 11 configurations of switch with thickness 1.2 μm.

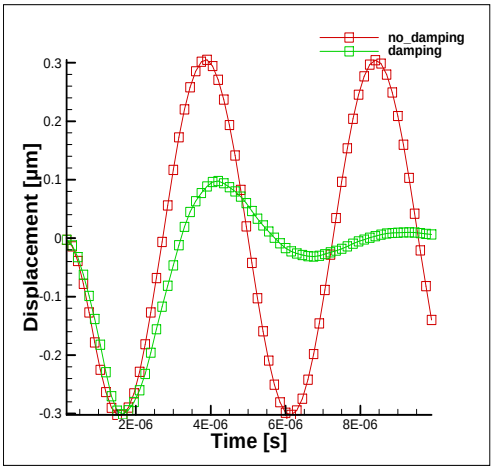

(a) Dimension 30 ×30

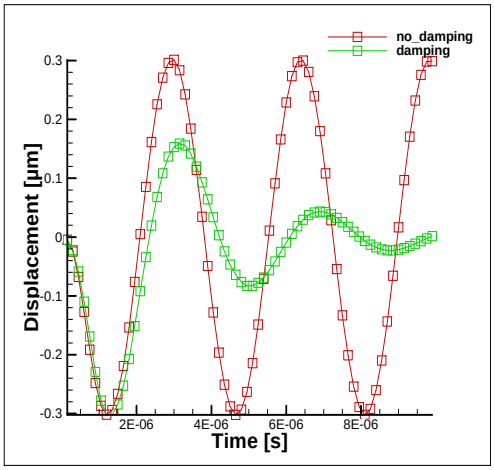

(b) Dimension 26 ×26

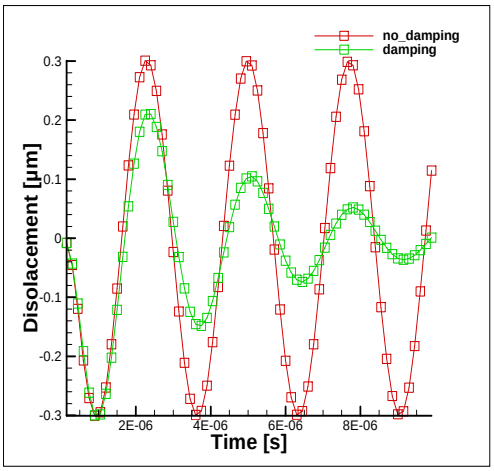

(c) Dimension 22 ×22

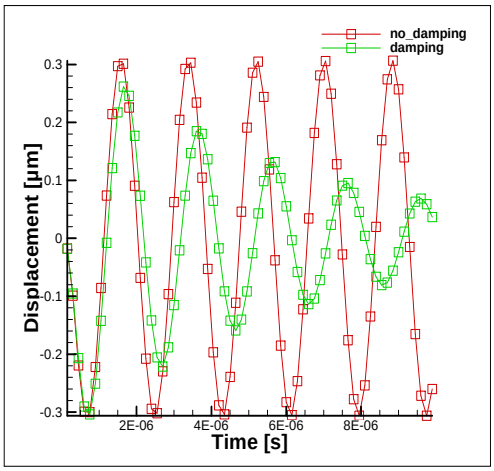

(d) Dimension 18 ×18

Figure 6.11: Comparison of damping with no damping of four configurations of switch with thickness 1.2 μm.

In the case of switch with thickness 1.2 μm, switching time shows the very same trend as previous cases. From switching time results, it is seen that switching time becomes smaller with decrease of dimension. Damped switching time is very similar to the undamped switching time in case of small dimension but for large dimension, discrepancy between undamped and damped switching time is noticeable. The re-

sponse of undamped and damped condition of four configurations have been shown in Figure 6.11. It is clear from figure that amplitude of response of under damped switch decreases with time. Under damped condition, the tip of switch makes only one contact with transmission pad or contact electrode during first cycle. From second cycle, amplitude starts to decrease. Squeeze film damping causes amplitude reduction but frequency of switch remains same.

6.3.3 Contact Force

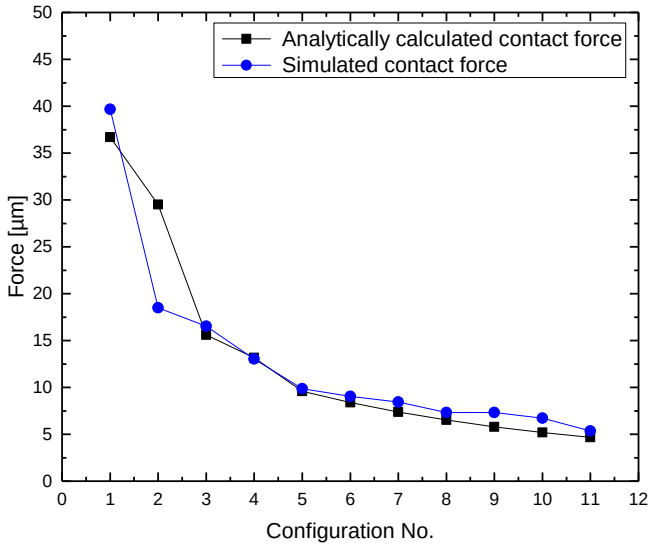

Figure 6.12: Analytic and simulated contact force of 11 configurations of switch with thickness 1.2 μm.

Actuation force, analytically calculated contact force, simulated contact force and contact resistance of 11 configurations of MEMS switch with thickness 1.2μm at applied voltage of 1.5 V_{PI} have been shown in Table 6.10. In case of switch with thickness 1.2 μm, simulated contact force for each configuration agrees with analytically calculated contact force. For each configuration, contact force is around 30-60% of actuation or pull-down force. Compared with thickness 1.6 μm and 1.4 μm, contact force has been decreased for each configuration. This decrease can be explained by attributing thickness reduction. Thickness reduction has decreased pull-in voltage

which results reduction in applied voltage of 1.5 V_{PI}. As a result, smaller actuation force has been generated than case 1 and case 2 which in turn causes in smaller contact force than case 1 and case 2. Contact resistance has decreased with increase of contact force as predicted by equation (4.36). Compared with case 1 and case 2, contact resistance reduced due to reduction in contact force.

Table 6.10: Actuation force, analytically calculated contact force, CoventorWare simulated contact force and contact resistance at 1.5 V_{PI} of 11 configurations of switch with thickness 1.2 μm.

Configuration No.	Actuation force (μN) at $1.5V_{PI}$	Analytically calculated contact force (μN) at $1.5V_{PI}$	CoventorWare simulated contact force (μN) at $1.5V_{PI}$	Contact resistance (Ω)
1	123.79	36.70	39.67	0.134
2	97.78	29.52	18.5	0.145
3	51.06	15.60	16.52	0.205
4	42.67	13.16	13.02	0.223
5	30.91	9.59	9.85	0.261
6	26.94	8.40	9.06	0.279
7	23.60	7.39	8.43	0.297
8	20.79	6.53	7.33	0.316
9	18.43	5.8	7.31	0.335
10	16.42	5.18	6.73	0.355
11	14.72	4.66	5.36	0.375

6.4 Case 4: Cantilever Beam with Thickness 1 μm

6.4.1 Pull-in Voltage(V_{PI})

3D CoventorWare simulated pull-in voltage of 11 configurations of switch with hole having thickness 1 μm have been shown in Table 6.11. Compare to case 1, case 2 and case 3, pull-in voltage has decreased in each configuration. This decrease is the

direct effect of reduction in thickness of the beam. Stiffness of beam is proportional to thickness of beam. Reduction of thickness decreases stiffness of beam. Again pull-in voltage is proportional to beam stiffness. As results, reduction of thickness has caused decrease in pull-in voltage.

Table 6.11: CoventorWare simulated pull-in voltage of 11 configurations of switch with thickness 1 μm.

Configuration No.	CoventorWare simulated pull-in voltage, (V) 3D model
1	120.31
2	62.50
3	45.31
4	36.86
5	26.56
6	21.88
7	18.44
8	15.63
9	13.47
10	11.56
11	10.12

6.4.2 Switching Time

Simulated damped and undamped switching time of MEMS switches with thickness 1 μm have been shown in Table 6.12. In the case of switch with thickness 1 μm, switching time shows the very same trend as previous cases. Configuration 10 and 11 do not get any contact at $1.5V_{PI}$, hence no switching time. From switching time results, it is seen that switching time becomes smaller with decrease of dimension.

Table 6.12: Damped and undamped switching time of 11 configurations of switch with thickness 1 μm.

Configuration No.	Switching time at $1.5V_{PI}$ without damping (μs)	Switching time at $1.5V_{PI}$ with damping (μs)
1	0.15	0.15
2	0.3	0.36
3	0.44	0.442
4	0.59	0.592
5	0.75	0.84
6	0.87	0.89
7	0.97	1.04
8	1.135	1.17
9	1.303	1.42
10	No contact	No contact
11	No contact	No contact

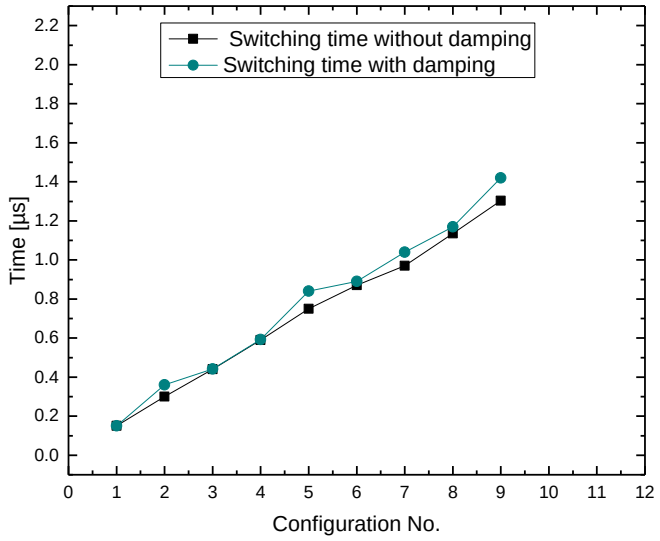

Figure 6.13: Damped and undamped switching time of 9 configurations of switch with thickness 1 μm.

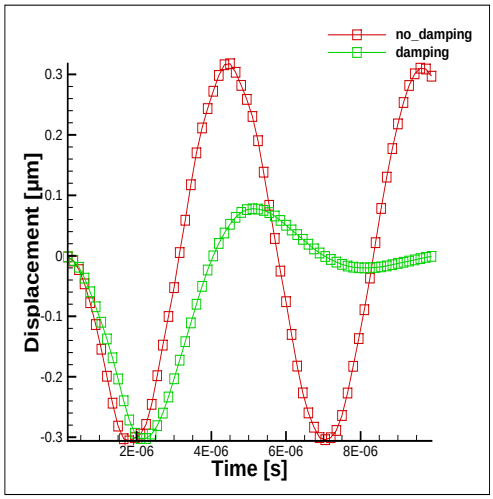

(a) Dimension 30 ×30

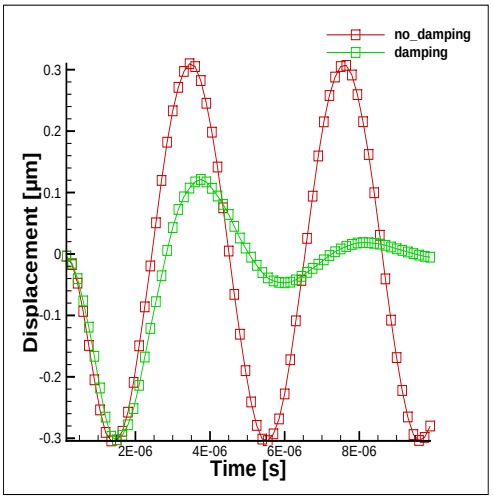

(b) Dimension 26 ×26

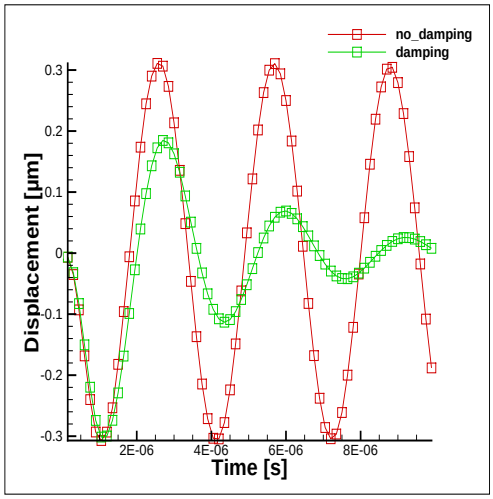

(c) Dimension 22 ×22

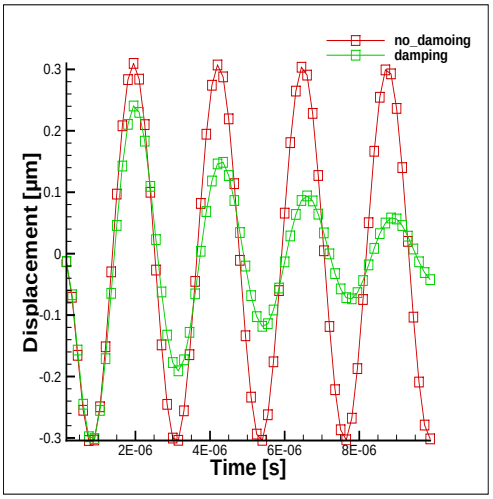

(d) Dimension 18 ×18

Figure 6.14: Comparison of damping with no damping of four configurations of switch with thickness 1 μm.

Damped switching time is very similar to the undamped switching time in case of small dimension but for large dimension, discrepancy between undamped and damped switching time is noticeable. Only configuration 1 gives same switching time for damped and undamped condition but rest of the configurations give remarkable difference between damped and undamped condition. This can be attributed to low actuation force because of low pull-in voltage as compared to previous cases. Because as actuation force gets smaller, damping force exerts more influence on dynamic be-

havior. The response of undamped and damped condition of four configurations have been shown in Figure 6.14. It is clear from figure that amplitude of response of under damped switch decreases with time. Under damped condition, the tip of switch makes only one contact with transmission pad or contact electrode during first cycle. From second cycle, amplitude starts to decrease. Squeeze film damping causes amplitude reduction but frequency of switch remains same.

6.4.3 Contact Force

Table 6.13: Actuation force, analytically calculated contact force, CoventorWare simulated contact force and contact resistance at $1.5V_{PI}$ of 11 configurations of switch with thickness 1 μm.

Configuration No.	Actuation force (μN) at $1.5V_{PI}$	Analytically calculated contact force (μN) at $1.5V_{PI}$	CoventorWare simulated contact force (μN) at $1.5V_{PI}$	Contact resistance (Ω)
1	123.79	36.70	22.94	0.134
2	61.58	18.59	11.22	0.186
3	29.55	9.03	9.72	0.269
4	24.70	7.61	7.73	0.293
5	17.89	5.55	5.58	0.343
6	15.60	4.86	5.92	0.367
7	13.66	4.27	4.86	0.391
8	12.03	3.78	4.73	0.416
9	10.66	3.36	3.86	0.441
10	9.50	No contact	No contact	No contact
11	8.52	No contact	No contact	No contact

Actuation force, analytically calculated contact force, simulated contact force and contact resistance of 11 configurations of MEMS switch with thickness $1\mu m$ at applied voltage of $1.5V_{PI}$ have been shown in Table 6.13. Actuation force and contact force have been determined at $1.5V_{PI}$ in order to get stable contact. In case of thick-

ness 1 μm, simulated contact force for each configuration agrees with analytically calculated contact force. Configuration 10 and 11 do not get any contact at $1.5V_{PI}$. For each configuration, contact force is around 30-60% of actuation or pull-down force. Compared with thickness 1.6 μm, 1.4 μm and 1.2 μm, contact force has decreased for each configuration. This decrease can be explained by attributing thickness reduction. Thickness reduction has decreased pull-in voltage which results reduction in applied voltage of $1.5V_{PI}$. As a result, smaller actuation force has been generated than case 1, case 2 and case 3 which in turn causes smaller contact force than case 1, case 2 and case 3. Contact resistance has been decreased with increase of contact force as predicted by equation (4.36). Compared to case 1, case 2 and case 3, contact resistance has been reduced due to reduction in contact force.

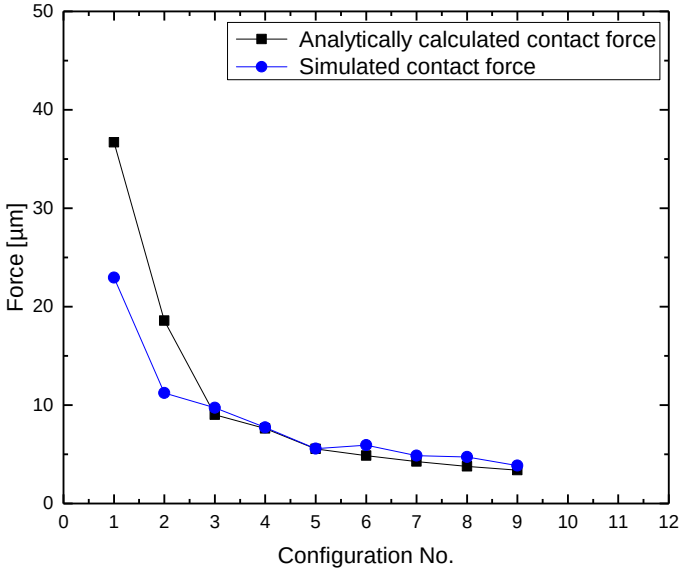

Figure 6.15: Analytic and simulated contact force of 11 configurations of switch with thickness 1 μm.

6.5 Results Comparison with Literature

6.5.1 Pull-in Voltage Results

Pull-in voltage results of different designs of gold made MEMS cantilever beam contact switches from literature have been mentioned in Table 6.14.

Table 6.14: Pull-in voltage results of different designs of MEMS switch from literature.

Literature	Switch dimension $(l_s \times w_s \times t_s)$	Hole dimension $(l_h \times w_h)$	$g(\mu m)$	$V_{PI}(V)$
[15]	$190 \times 160 \times 5\mu m$	$70 \times 50\mu m$	1.2	12.2
[16]	$135 \times 130 \times 12\mu m$	No hole	0.85	64
[14]	$24 \times 25 \times 1.6\mu m$	$8 \times 15\mu m$	0.5	34
[17]	$200 \times 64 \times 5\mu m$	No hole	1.7	27.65
[17]	$200 \times 52 \times 5\mu m$	No hole	1.7	26.37

l_s: length of switch, w_s: width of switch, t_s: thickness of switch, l_h: length of hole, w_h: width of hole, g: gap between electrodes, V_{PI}: pull-in voltage.

Literature [15], [16] and [17] reported low pull-in voltage with large dimension of switch. In all literature, large length switch was modeled which subsequently reduced stiffness of switches. As mentioned earlier that pull-in voltage is proportional to beam stiffness; this fact caused low pull-in voltage. Another reason behind low pull-in voltage is that large dimension ensured large actuation area. Since pull-in voltage is inversly proportional to actuation area, hence low pull-in voltage. In this study, length and width have been limited between 10 μm to 30 μm for miniaturization purpose, thus high stiffness and low actuation area has been generated in first 5 configurations. Configurations from 6 to 11 have provided better result in comparison with literature. Configurations from 6 to 8 have given nearly same pull-in voltage in comparison with dimension of switches of literature, whereas configurations from 9 to 11 have given less pull-in voltage compared with literature. The main reasons behind low pull-in voltage, despite small switch dimension compared to literature, are small thickness

of beam and small width at anchor point. Literature [14] tested same dimension of switch as configuration 8 of case 1 and measured pull-in voltage of 34 V, whereas pull-in voltage has been found for configuration 8 as 30.31 V in this study. Therefore, pull-in voltage results from configuration designed in this study agree with literature and some configurations provide better pull-in voltage compared to literature.

6.5.2 Contact Force Results

Contact force results of different designs of gold made MEMS cantilever beam contact switch from literature have been mentioned in Table 6.15. Contact forces were calculated at $1.5V_{PI}$. Literature [15], [16], [10] and [41] reported high contact force compared with this study but their switch dimension was many times higher than switches designed in this study. Large dimension of switch provided large actuation area, hence large actuation or pull down force. This high pull down force resulted in high contact force, since contact force is around 30-60% of actuation or pull-down force. In this study, switch dimensions are small for the sake of miniaturization; hence small actuation area are available for actuation.

Table 6.15: Contact force results of different designs of MEMS switch from literature.

Literature	Switch dimension $(l_s \times w_s \times t_s)$	Hole dimension $(l_h \times w_h)$	$A(\mu m^2)$	$g(\mu m)$	$F_c(\mu N)$
[15]	$190 \times 160 \times 5\mu m$	$70 \times 50\mu m$	8000	1.2	220 at 20 V
[16]	$135 \times 130 \times 12\mu m$	No hole	17550	0.85	800 at 90 V
[14]	$24 \times 25 \times 1.6\mu m$	$8 \times 15\mu m$	440	0.5	15.2 at 51 V
[10]	$170 \times 147 \times 6.5\mu m$	No hole	11050	1.2	610 at 68 V
[41]	$400 \times 75 \times 4.3\mu m$	No hole	11250	3.2	35.5 at 40 V

l_s: length of switch, w_s: width of switch, t_s: thickness of switch, l_h: length of hole, w_h: width of hole,

As a result, low contact force has been generatde compared with the contact forces found in literature. Literature [14] analyzed the similar dimension of switch as configuration 8 of case 1 and reported a contact force of 15.5 μN. This results is good consistent with result of this work. In configuration 8, contact force has been found as

15.48 μN from analytic solution and 16.33 μN from simulation. Therefore, considering miniaturization of switch, it can be said that contact forces of switches designed in this study are good consistent with literature.

6.5.3 Switching Time Results

Switching time results of different gold made MEMS cantilever beam contact switches from literature have been mentioned in Table 6.16. Literature [16], [10], [17] and [14] reported large switching time in comparison with this work in spite of having nearly same pull-in voltage. Switching time not only depends on pull-in voltage but also depends on the quality factor of beam $Q = K/\omega_0 b$; where K is stiffness of beam, ω_0 is resonant frequency of beam and b is the damping co-efficient. Large quality factor ensures low switching time. The value of Q less than 0.5 results in large switching time [23].

Table 6.16: Switching time results of different designs of MEMS switch from literature.

Literature	Switch dimension ($l_s \times w_s \times t_s$)	Hole dimension ($l_h \times w_h$)	$g(\mu m)$	$V_{PI}(V)$	$t_s(\mu m)$
[16]	$135 \times 130 \times 12 \mu m$	No hole	0.85	64	6.4
[17]	$200 \times 64 \times 5 \mu m$	No hole	1.7	27.65	21.31
[10]	$170 \times 147 \times 6.5 \mu m$	No hole	1.2	35	< 10
[17]	$200 \times 52 \times 5 \mu m$	No hole	1.7	26.37	30.85
[14]	$24 \times 25 \times 1.6 \mu m$	$8 \times 15 \mu m$	0.5	34	1.1

l_s: length of switch, w_s: width of switch, t_s: thickness of switch, l_h: length of hole, w_h: width of hole, g: gap between electrodes, V_{PI}: pull-in voltage and t_s: switching time.

Large dimension decreases K and increases damping effect b which in turn decreases quality factor Q, and hence switching time becomes larger. Each lietarute designed large size of switch, thus quality factor decreased. This decrease in quality factor increased switching time. Large gap also causes increase in switching time. Small

gap ensures large actuation force which results in low switching time. In this thesis, for miniaturization, both length and width of the beam have been limited from 10 μm to 30 μm which has provided higher Q. Gap has been fixed small as 0.5 μm which is another reason for obtaining low switching time. In literature [14] nearly same dimension of switch as configuration 8 of case 1 was tested and found switching time of 1.1 μs, whereas nearly same switching time of configuration 8 has been found in this work as 0.90 μs. Therefore, considering all facts, switches designed in this study provide better switching time in comparison with literature.

From comparison, it is seen that each author analyzed MEMS contact switch for specific performance criterion. No author has addressed the issue of miniaturization and three performance criteria simultaneously. This thesis has successfully addressed the all issues simultaneously which previously was not done. This thesis has analyzed the performance criteria of MEMS switch at very small dimension and reported good results compared with literature.

CHAPTER 7

OPTIMIZATION OF SHAPE OF MEMS CANTILEVER SWITCH

MEMS switch optimization in this work can be recapitulated as follows:

- Given: in this study, mechanical, electrical, thermal properties of switch's materials are given. Topology of switch and dimple, dimension of dimple and gap between beam and down electrodes are also fixed.
- Objective: the objective of this work is to find out an optimized shape of MEMS cantilever beam contact switch for miniaturization.
- Minimization: pull-in voltage and switching time have to be minimized.
- Maximization: contact force has to be maximized.

7.1 Case 1 : Thickness 1.6 μm

Simulated pull-in voltage, contact force, and switching time results of switch with hole having thickness 1.6 μm have been mentioned in Table 7.1. Contact force versus pull-in voltage, switching time versus pull-in voltage, switching time versus contact force graphs have been projected in Figure 7.1. It has been already mentioned that the main purpose of this work is to find out an miniature optimized shape of MEMS cantilever beam contact switches for low pull-in voltage, small switching time and large contact force. Bearing these criteria in mind, from Figure 7.1 it is seen that configuration 7 with dimension $22 \times 22 \mu m$ is the most promising candidate compared to other configurations.

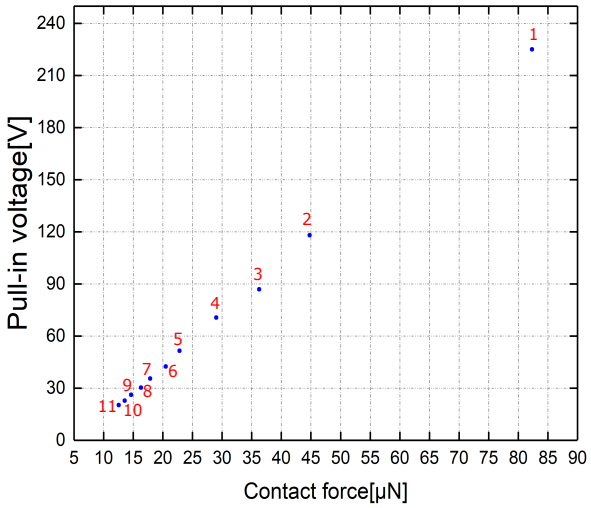

(a)

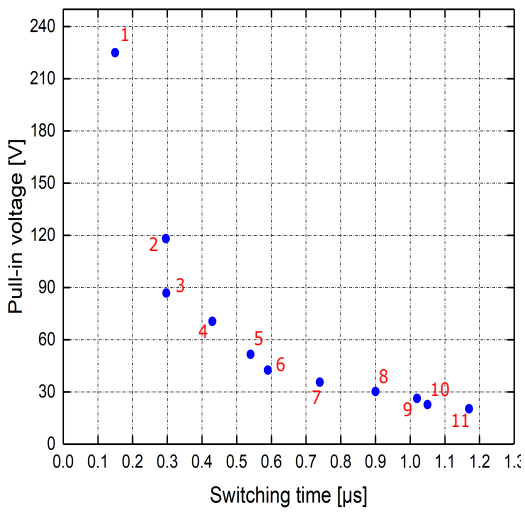

(b)

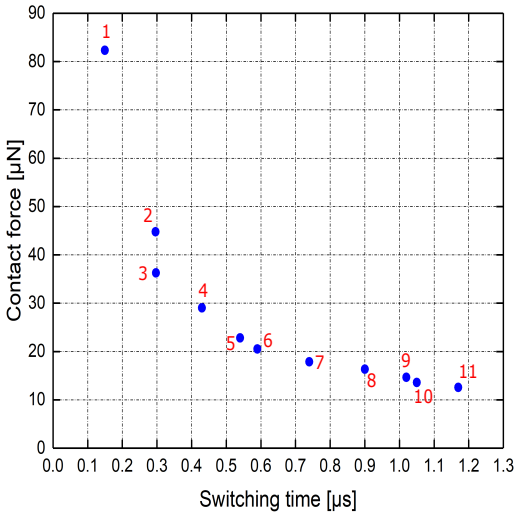

(c)

Figure 7.1: Results of 9 configurations of switch with thickness 1.6 μm are projected: (a) contact force versus pull-in voltage, (b) switching time versus pull-in voltage, (c) switching time versus contact force.

It gives pull-in voltage of 35.62 V which is very low considering dimension, contact force of 17.87 μN which is above the contact force for stable MEMS switch operation of 15.5 μN found in [14] and switching time of 0.74 μs which is lower than the

results of switch developed for RF application in [14] for dimension $24 \times 24\mu m$. For configurations 1 to 6, although switching time is very small and contact force is large but pull-in voltage is comparatively large. For configurations 8 to 11, although pull-in voltage and switching time is small but contact force is very small for stable switch operation. Therefore, from the discussion it can be concluded that configuration 7 with dimension $22 \times 22\mu m$ is the optimized miniature shape of switch with thickness 1.6 μm.

Table 7.1: Results of switch with thickness 1.6 μm .

Configuration No.	$D_b(l_s \times w_s)$	$V_{PI}(V)$	$F_c(\mu N)$	$t(\mu s)$
1	$10 \times 10\mu m$	225	82.33	0.15
2	$12 \times 12\mu m$	118.13	44.79	0.296
3	$14 \times 14\mu m$	86.88	36.27	0.297
4	$16 \times 16\mu m$	70.62	29.02	0.43
5	$18 \times 18\mu m$	51.56	22.81	0.54
6	$20 \times 20\mu m$	42.50	20.51	0.59
7	$22 \times 22\mu m$	35.62	17.81	0.74
8	$24 \times 24\mu m$	30.31	16.33	0.90
9	$26 \times 26\mu m$	26.25	14.67	1.02
10	$28 \times 28\mu m$	22.81	13.58	1.05
11	$30 \times 30\mu m$	20.31	12.56	1.17

D_b: dimension of beam, V_{PI}: pull-in voltage, F_c: contact force, t: switching time.

7.2 Case 2 : Thickness 1.4 μm

Simulated pull-in voltage, contact force and switching time results of switch with hole having thickness 1.4 μm have been mentioned in Table 7.2. Contact force versus pull-in voltage, switching time versus pull-in voltage, switching time versus contact force graphs have been projected in Figure 7.2. It shows that only configuration 5 gives reasonable pull-in voltage, switching time and contact force compared to other configurations. It gives pull-in voltage of 42.81 V, switching time of 0.59 μs, contact

force of 15.60 μN.

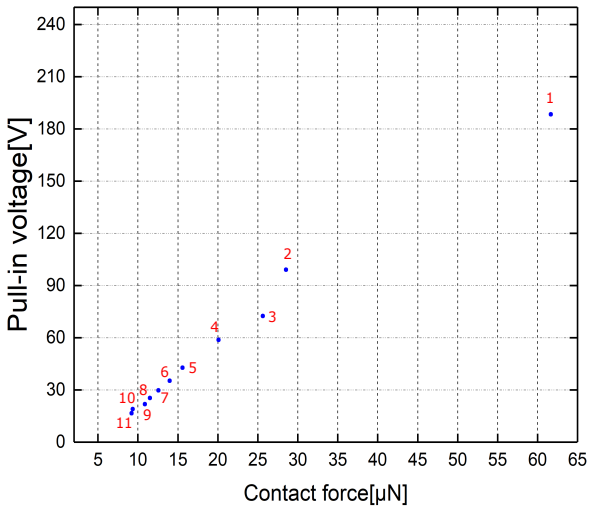

(a)

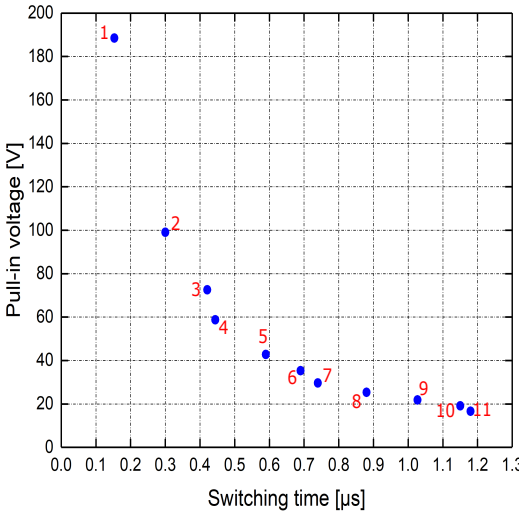

(b)

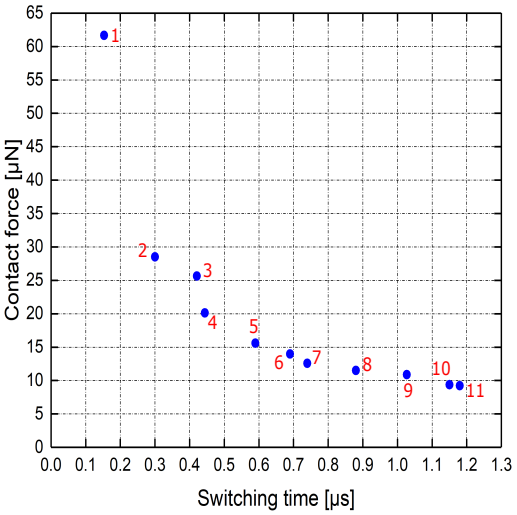

(c)

Figure 7.2: Results of 9 configurations of switch with thickness 1.4 μm are projected: (a) contact force versus pull-in voltage, (b) switching time versus pull-in voltage, (c) switching time versus contact force.

In contrast, configurations from 1 to 4 give very high pull-in voltage although switch-

ing time is small and contact force is large. High pull-in voltage increases operation voltage which violates the low pull-in voltage criterion of MEMS switch for commercial applications. Becuase communication system and radar system require very low operation volatge. Configurations from 6 to 11 give very low contact force although pull-in voltage and switching time are low. Minimum contact force has been reported in [14] as 15.5 μN for stable contact. These configurations give maximum contact force as 13.97 μN which is below the contact force found in [14]. Therefore, from the discussion it can be concluded that configuration 5 with dimension $18 \times 18 \mu m$ is the optimized miniature shape of switch with thickness 1.4 μm.

Table 7.2: Results of switch with thickness 1.4 μm.

Configuration No.	$D_b(l_s \times w_s)$	$V_{PI}(V)$	$F_c(\mu N)$	$t_s(\mu s)$
1	$10 \times 10 \mu m$	188.43	61.67	0.153
2	$12 \times 12 \mu m$	99.06	28.52	0.30
3	$14 \times 14 \mu m$	72.50	25.64	0.421
4	$16 \times 16 \mu m$	58.75	20.10	0.444
5	$18 \times 18 \mu m$	42.81	15.60	0.59
6	$20 \times 20 \mu m$	35.31	13.97	0.69
7	$22 \times 22 \mu m$	29.69	12.57	0.74
8	$24 \times 24 \mu m$	25.31	11.51	0.88
9	$26 \times 26 \mu m$	21.87	10.89	1.027
10	$28 \times 28 \mu m$	19.06	9.36	1.15
11	$30 \times 30 \mu m$	16.56	9.21	1.18

D_b: dimensions of beam, V_{PI}: pull-in voltage, F_c: contact force, t_s: switching time.

7.3 Case 3 : Thickness 1.2 μm

Simulated pull-in voltage, contact force and switching time results of switch with hole having thickness 1.2 μm have been mentioned in Table 7.3. Contact force versus pull-in voltage, switching time versus pull-in voltage, switching time versus contact force graphs have been projected in Figure 7.3. Results show that none of the configuration

gives reasonable pull-in voltage, switching time and contact force. Configuration 1, 2 and 3 give reasonable contact force but pull-in is very high which violates the criterion of low operation voltage. Configurations

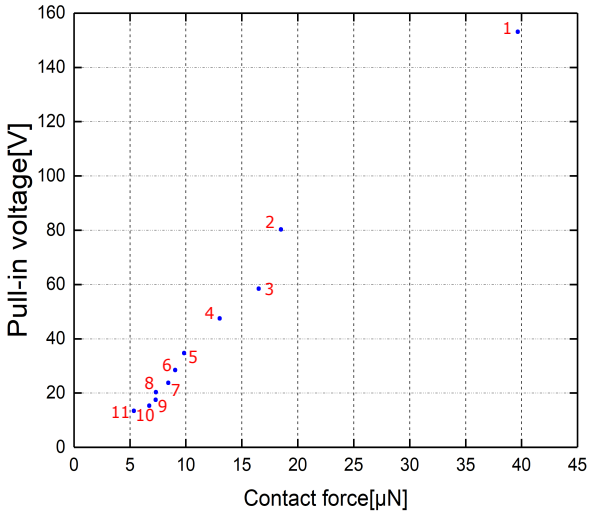

(a)

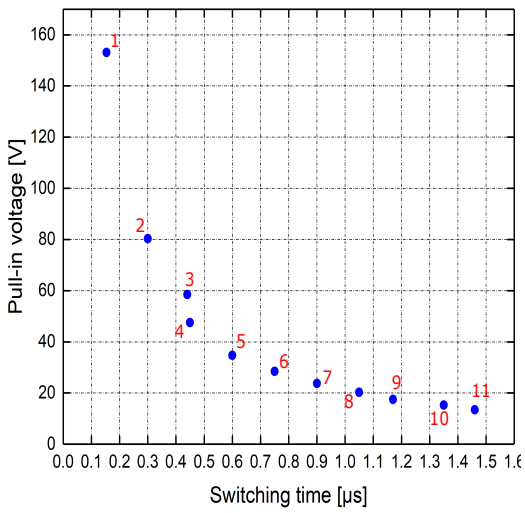

(b)

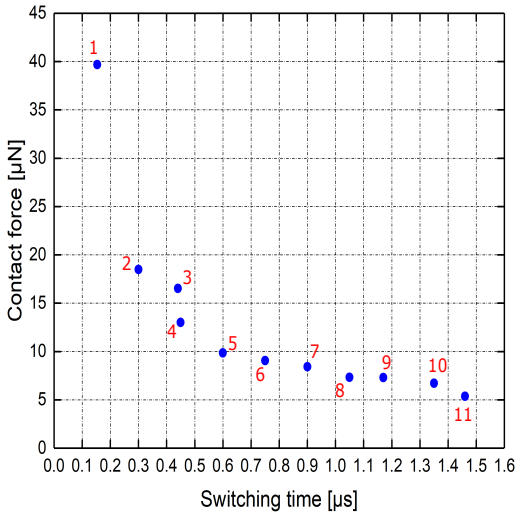

(c)

Figure 7.3: Results of 9 configurations of switch with thickness 1.2 μm are projected: (a) contact force versus pull-in voltage, (b) switching time versus pull-in voltage, (c) switching time versus contact force.

from 4 to 11 give reasonable pull-in voltage but contact force is not sufficient for stable switch operation. Minimum contact force has been reported in [14] as 15.5 μN for stable contact. These configurations give maximum contact force as 13.02 μN which is below the contact force found in [14]. Therefore, based on the results it can be concluded that cantilever beam contact switches with thickness 1.2 μs are not suitable for MEMS application with dimensions studied in this work.

Table 7.3: Results of switch with thickness 1.2 μm.

Configuration No.	$D_b(l_s \times w_s)$	$V_{PI}(V)$	$F_c(\mu N)$	$t_s(\mu s)$
1	$10 \times 10 \mu m$	153.12	39.67	0.154
2	$12 \times 12 \mu m$	80.31	18.50	0.30
3	$14 \times 14 \mu m$	58.44	16.52	0.44
4	$16 \times 16 \mu m$	47.50	13.02	0.45
5	$18 \times 18 \mu m$	34.69	9.85	0.60
6	$20 \times 20 \mu m$	28.44	9.06	0.75
7	$22 \times 22 \mu m$	23.75	8.43	0.90
8	$24 \times 24 \mu m$	20.31	7.33	1.05
9	$26 \times 26 \mu m$	17.50	7.31	1.17
10	$28 \times 28 \mu m$	15.31	6.73	1.35
11	$30 \times 30 \mu m$	13.44	5.36	1.46

D_b: dimensions of beam, V_{PI}: pull-in voltage, F_c: contact force, t_s: switching time.

7.4 Case 4 : Thickness 1 μm

Simulated pull-in voltage, contact force and switching time results of switch with thickness 1 μm have been mentioned in Table 7.4. Contact force versus pull-in voltage, switching time versus pull-in voltage, switching time versus contact force graphs have been projected in Figure 7.4. Results show that none of the configuration gives reasonable pull-in voltage, switching time and contact force. Configuration 1 gives reasonable contact force but pull-in voltage is extremely high. High pull-in voltage requires high actuation voltage which violates the low pull-in voltage requirement.

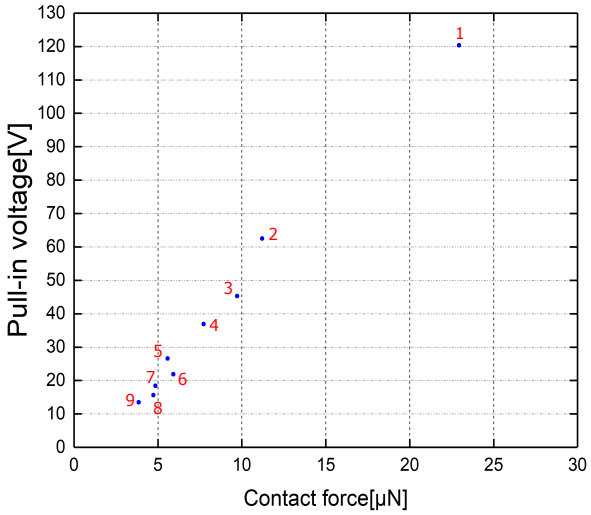

(a)

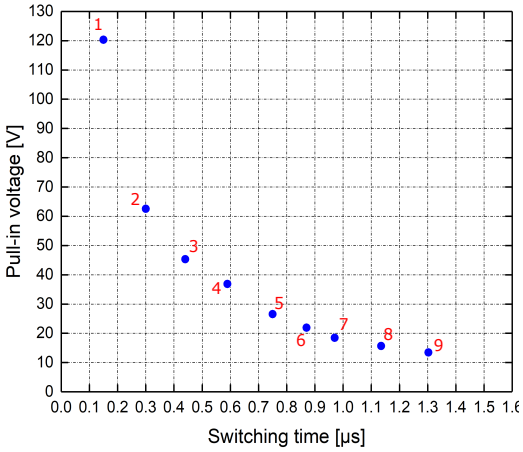

(b)

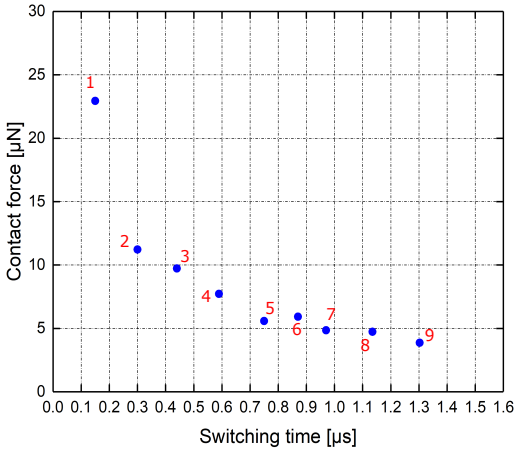

(c)

Figure 7.4: Results of 9 configurations of switch with thickness 1 μm are projected: (a) contact force versus pull-in voltage, (b) switching time versus pull-in voltage, (c) switching time versus contact force.

MEMS switches relaibale operation voltage lise between 20-80 V [1]. It gives pull-in voltage 120.31 V. Configurations from 2 to 11 give reasonable pull-in voltage but contact force is very small. Minimum contact force has been reported in [14] as 15.5 μN for stable contact. These configurations give maximum contact force as 11.06

μN which is below the contact force found in [14]. Therefore, based on the results it can be concluded that cantilever beam contact switches with thickness 1 μm are not suitable for MEMS application with dimensions studied in this work.

Table 7.4: Results of switch with thickness 1 μm.

Configuration No.	$D_b(l_s \times w_s)$	$V_{PI}(V)$	$F_c(\mu N)$	$t_s(\mu s)$
1	$10 \times 10 \mu m$	120.31	22.94	0.15
2	$12 \times 12 \mu m$	62.50	11.22	0.36
3	$14 \times 14 \mu m$	45.31	9.72	0.44
4	$16 \times 16 \mu m$	36.86	7.73	0.59
5	$18 \times 18 \mu m$	25.56	5.58	0.84
6	$20 \times 20 \mu m$	21.88	5.92	0.89
7	$22 \times 22 \mu m$	18.44	4.86	1.04
8	$24 \times 24 \mu m$	15.63	4.73	1.17
9	$26 \times 26 \mu m$	13.47	3.86	1.42
10	$28 \times 28 \mu m$	11.56	No contact	No contact
11	$30 \times 30 \mu m$	10.12	No contact	No contact

D_b: dimensions of beam, V_{PI}: pull-in voltage, F_c: contact force, t_s: switching time.

The following Table 7.5 summarizes the optimized shape of MEMS switches with four different thickness.

Table 7.5: Optimized shape of four cases.

Thickness (μm)	Configuration No.	Dimension	$V_{PI}(V)$	$F_c(\mu N)$	$t_s(\mu s)$
1.6	7	$22 \times 22 \mu m$	35.62	17.81	0.74
1.4	5	$18 \times 18 \mu m$	42.81	15.60	0.59
1.2	no configuration found for optimization.				
1	no configuration found for optimization.				

CHAPTER 8

CONCLUDING REMARKS AND FUTURE WORKS

In this thesis, 44 configurations of gold made MEMS cantilever contact switch have been critically analyzed in order to find out miniature optimized shape for low pull-in voltage, low switching time and high contact force. Mechanical and electrical mechanisms related to MEMS switches operation have also been demonstrated in this work. Low pull-in voltage ensures low power consumption which is essential for commercial and military applications specially for space or wireless systems. Low switching time provides faster operation facility of switch which is essential for communication system. High contact force ensures stable operation of switches. 44 configurations have been categorized into four cases based on thickness of beam. Squeeze film damping effect on switch dynamic operation has been evaluated. Pull-in voltage, switching time and contact force for each configuration have been evaluated in 3D MEMS analysis software CoventorWare. Results obtained from CoventorWare have been validated with analytically calculated results. CoventorWare results have also been compared with literature. According to obtained results, introduction of rectangular hole at the anchor point significantly reduces pull-in voltage. Introduction of hole also diminishes the inertia effect in beam which in turn also lowers the switching time. It has been observed that pull-in voltage increases with decrease of beam length and increase of thickness of beam. Switching time becomes lower with decrease of beam length and increase of thickness of beam. Contact force also shows the same behavior as switching time.

The results of this study show that for switch with thickness 1.6 μm, configuration 7 with dimension $22 \times 22 \mu m$ provides miniature optimized shape to obtain low pull-in voltage, small switching time and high contact force for stable switch operation.

Other configurations do not give satisfactory results for all three criteria. Large length switches give satisfactory low pull-in voltage and switching time but contact force is very small which can not ensure stable operation. Low length switches give satisfactory contact force and switching time but pull-in voltage is very high for MEMS application. In case 2, switch with thickness 1.4 μm, configuration 5 with dimension $18 \times 18 \mu m$ gives satisfactory pull-in voltage, switching time and contact force. Other configurations lack behind the desired requirement of any of one criterion from pull-in voltage, switching time and contact force. In case 3 and 4, switches with thickness 1.2 μm and 1 μm , no configuration provides satisfactory results for MEMS application. Any of one criterion from pull-in voltage, switching time and contact force does not satisfy the desired requirement for stable switch operation. Therefore, it can be seen that cantilever beam based MEMS contact switch shows poor performance with the decrease of thickness. Switch with thickness below 1.4 μm shows very poor performance for stable MEMS switch operation.

The future steps to continue the work are that to fabricate the miniature optimized shape and experimentally obtain the results. Other materials made switches can also be analyzed to validate the conclusions found by this work.

REFERENCES

[1] G. M. Rebeiz and J. B. Muldavin, "Rf mems switches and switch circuits," *IEEE Microwave magazine*, vol. 2, no. 4, pp. 59–71, 2001.

[2] P. M. Zavracky, S. Majumder, and N. E. McGruer, "Micromechanical switches fabricated using nickel surface micromachining," *Journal of Microelectromechanical Systems*, vol. 6, no. 1, pp. 3–9, 1997.

[3] E. R. Brown, "Rf-mems switches for reconfigurable integrated circuits," *IEEE Transactions on microwave theory and techniques*, vol. 46, no. 11, pp. 1868–1880, 1998.

[4] K. Petersen, "Micromechanical membrane switches on silicon," *IBM Journal of Research and Development*, vol. 23, no. 4, pp. 376–385, 1979.

[5] J. J. Yao, "Rf mems from a device perspective," *Journal of micromechanics and microengineering*, vol. 10, no. 4, p. R9, 2000.

[6] E. J. Kruglick and K. S. Pister, "Lateral mems microcontact considerations," *Journal of Microelectromechanical Systems*, vol. 8, no. 3, pp. 264–271, 1999.

[7] R. Holm, *Electric contacts: theory and application*. Springer Science & Business Media, 2013.

[8] X. Lafontan, F. Pressecq, G. Perez, C. Dufaza, and J.-M. Karam, "Physical and reliability issues in mems micro-relays with gold contacts," in *Proceedings of the SPIE—The International Society for Optical Engineering*, vol. 4558, p. 11, 2001.

[9] O. Rezvanian, M. Zikry, C. Brown, and J. Krim, "Surface roughness, asperity contact and gold rf mems switch behavior," *Journal of Micromechanics and Microengineering*, vol. 17, no. 10, p. 2006, 2007.

[10] H. Sedaghat-Pisheh and G. M. Rebeiz, "Variable spring constant, high contact force rf mems switch," in *Microwave Symposium Digest (MTT), 2010 IEEE MTT-S International*, pp. 304–307, IEEE, 2010.

[11] Y. Wang, Z. Li, D. T. McCormick, and N. C. Tien, "A micromachined rf microrelay with electrothermal actuation," *Sensors and Actuators A: Physical*, vol. 103, no. 1, pp. 231–236, 2003.

[12] I. Schiele, J. Huber, B. Hillerich, and F. Kozlowski, "Surface-micromachined electrostatic microrelay," *Sensors and Actuators A: Physical*, vol. 66, no. 1, pp. 345–354, 1998.

[13] H. Lee, R. A. Coutu, S. Mall, and K. D. Leedy, "Characterization of metal and metal alloy films as contact materials in mems switches," *Journal of Micromechanics and Microengineering*, vol. 16, no. 3, p. 557, 2006.

[14] R. Stefanini, M. Chatras, P. Blondy, and G. M. Rebeiz, "Miniature mems switches for rf applications," *Journal of Microelectromechanical Systems*, vol. 20, no. 6, pp. 1324–1335, 2011.

[15] N. Nishijima, J.-J. Hung, and G. M. Rebeiz, "A low-voltage high contact force rf-mems switch," in *Microwave Symposium Digest, 2004 IEEE MTT-S International*, vol. 2, pp. 577–580, IEEE, 2004.

[16] C. D. Patel and G. M. Rebeiz, "Rf mems metal-contact switches with mn-contact and restoring forces and low process sensitivity," *IEEE Transactions on Microwave Theory and Techniques*, vol. 59, no. 5, pp. 1230–1237, 2011.

[17] M. M. Shalaby, Z. Wang, L. L.-W. Chow, B. D. Jensen, J. L. Volakis, K. Kurabayashi, and K. Saitou, "Robust design of rf-mems cantilever switches using contact physics modeling," *IEEE Transactions on Industrial Electronics*, vol. 56, no. 4, pp. 1012–1021, 2009.

[18] S. Majumder, N. McGruer, P. M. Zavracky, G. G. Adams, R. H. Morrison, and J. Krim, "Measurement and modelling of surface micromachined, electrostatically actuated microswitches," in *Solid State Sensors and Actuators, 1997. TRANSDUCERS'97 Chicago., 1997 International Conference on*, vol. 2, pp. 1145–1148, IEEE, 1997.

[19] F. Ke, J. Miao, and J. Oberhammer, "A ruthenium-based multimetal-contact rf mems switch with a corrugated diaphragm," *Journal of microelectromechanical systems*, vol. 17, no. 6, pp. 1447–1459, 2008.

[20] D. Hyman, J. Lam, B. Warneke, A. Schmitz, T. Hsu, J. Brown, J. Schaffner, A. Walston, R. Y. Loo, M. Mehregany, *et al.*, "Surface-micromachined rf mems switches on gaas substrates," *International Journal of RF and Microwave Computer-Aided Engineering: Co-sponsored by the Center for Advanced Manufacturing and Packaging of Microwave, Optical, and Digital Electronics (CAMPmode) at the University of Colorado at Boulder*, vol. 9, no. 4, pp. 348–361, 1999.

[21] Z. Guo, N. McGruer, and G. Adams, "Modeling, simulation and measurement of the dynamic performance of an ohmic contact, electrostatically actuated rf mems switch," *Journal of Micromechanics and Microengineering*, vol. 17, no. 9, p. 1899, 2007.

[22] O. Bauchau and J. Craig, "Euler-bernoulli beam theory," in *Structural analysis*, pp. 173–221, Springer, 2009.

[23] G. M. Rebeiz, *RF MEMS: theory, design, and technology*. John Wiley & Sons, 2004.

[24] S. D. Senturia, *Microsystem design*. Springer Science & Business Media, 2007.

[25] M. Bao, *Analysis and design principles of MEMS devices*. Elsevier, 2005.

[26] A. H. Nayfeh, M. I. Younis, and E. M. Abdel-Rahman, "Dynamic pull-in phenomenon in mems resonators," *Nonlinear dynamics*, vol. 48, no. 1-2, pp. 153–163, 2007.

[27] S. Krylov and R. Maimon, "Pull-in dynamics of an elastic beam actuated by continuously distributed electrostatic force," *Journal of vibration and acoustics*, vol. 126, no. 3, pp. 332–342, 2004.

[28] M. Bao and H. Yang, "Squeeze film air damping in mems," *Sensors and Actuators A: Physical*, vol. 136, no. 1, pp. 3–27, 2007.

[29] T. Veijola, H. Kuisma, J. Lahdenperä, and T. Ryhänen, "Equivalent-circuit model of the squeezed gas film in a silicon accelerometer," *Sensors and Actuators A: Physical*, vol. 48, no. 3, pp. 239–248, 1995.

[30] G. De Pasquale and A. Soma, "Dynamic identification of electrostatically actuated mems in the frequency domain," *Mechanical systems and signal processing*, vol. 24, no. 6, pp. 1621–1633, 2010.

[31] S. S. Rao, *Vibration of continuous systems*. John Wiley & Sons, 2007.

[32] W. Thomson, *Theory of vibration with applications*. CRC Press, 1996.

[33] I. Chowdhury and S. P. Dasgupta, "Computation of rayleigh damping coefficients for large systems," *The Electronic Journal of Geotechnical Engineering*, vol. 8, no. 0, pp. 1–11, 2003.

[34] C. Inc, *CoventorWare Analyzer Reference:Section 7:DampingMM*. Coventor, 2014.

[35] H. Kwon, D.-J. Choi, J.-H. Park, H.-C. Lee, Y.-H. Park, Y.-D. Kim, H.-J. Nam, Y.-C. Joo, and J.-U. Bu, "Contact materials and reliability for high power rf-mems switches," in *Micro Electro Mechanical Systems, 2007. MEMS. IEEE 20th International Conference on*, pp. 231–234, IEEE, 2007.

[36] D. Hyman and M. Mehregany, "Contact physics of gold microcontacts for mems switches," in *Electrical Contacts, 1998. Proceedings of the Forty-Fourth IEEE Holm Conference on*, pp. 133–140, IEEE, 1998.

[37] H. Angus, "Surface films on precious-metal contacts," *British Journal of Applied Physics*, vol. 13, no. 2, p. 58, 1962.

[38] J. A. Greenwood, "Constriction resistance and the real area of contact," *British Journal of Applied Physics*, vol. 17, no. 12, p. 1621, 1966.

[39] F. Seitz, *The modern theory of solids*. McGraw-Hill Book Company, Inc; New York, 1940.

[40] M. Myers, M. Leidner, H. Schmidt, S. Sachs, and A. Baeumer, "Contact resistance reduction by matching current and mechanical load carrying asperity

junctions," in *Electrical Contacts (Holm), 2012 IEEE 58th Holm Conference on*, pp. 1–8, IEEE, 2012.

[41] R. A. Coutu Jr, P. E. Kladitis, L. Starman, and J. R. Reid, "A comparison of micro-switch analytic, finite element, and experimental results," *Sensors and Actuators A: Physical*, vol. 115, no. 2-3, pp. 252–258, 2004.